Radiolarian-based Quaternary palaeoclimate reconstructions of the Sabrina Coast, East Antarctica.

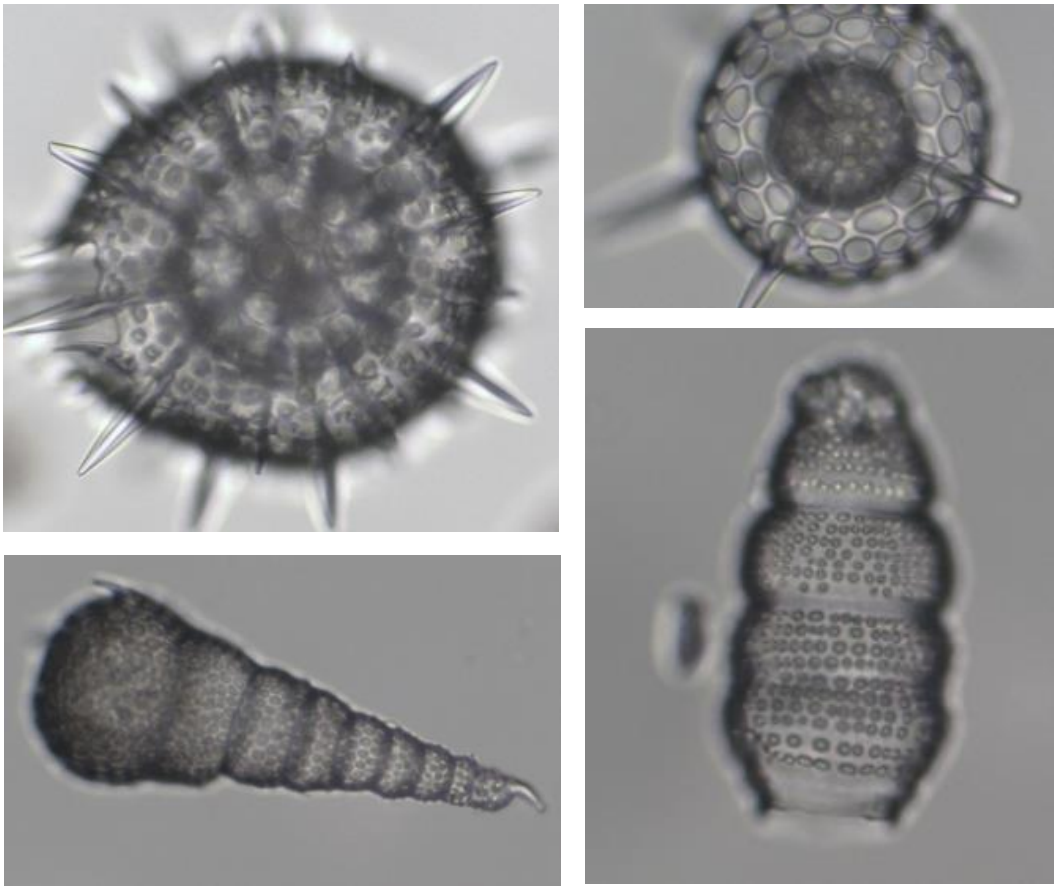

Kelly-Anne Lawler

A thesis submitted in fulfilment of the requirements for the Degree of Master of Research in Biological Sciences.

This thesis is written in the form of a journal article from Quaternary Australasia with exceptions that figures are embedded into body as opposed to being contained in separate files, figure captions appear with relevant figures as opposed to being contained at end of body text and spacing is 1.5x, all as requested by Macquarie University.

Declaration

I wish to acknowledge the following assistance in the research detailed in this report:

N/A

All research described in this report is my own original work.

Kelly-Anne Lawler

20 November 2018

ACKNOWLEDGEMENTS

Many thanks go to:

My project supervisors, Dr Giuseppe Cortese (GNS Science) & Dr Matthew Kosnik (Macquarie University), for teaching me everything they know, and some of it sticking!

The crew and science party of voyage IN2017_V01, in particular, chief scientist A/Prof Leanne Armand. Thanks also go to Dr Linda Armbrecht, Dr Amy Leventer, Dr Bradley Opdyke, Dr Phil O'Brien & Dr Alix Post, as well as Dimitris Evangelinos, Liam Holder, Rushi Perera, Vanessa Pirotta and Sarah Tynan for being great company onboard.

Giuseppe Cortese & Meera Sood, Melanie Gibbons & Simon Arnold and Sarah Thornton & Roy Forsyth for providing me with a home away from home, delicious meals and personal taxi services in Wellington, Canberra and Hobart.

The Macquarie University Palaeobiology Lab, Marine and Coastal Phytoplankton Lab, Dr Anthony Chariton for use of his lab space and my Macquarie University colleagues who have been great gym, burrito and beer buddies.

My non-sciencey husband, Iliyan Darganov, and friends who have been a great support and listened patiently to me raving on about things in which they probably have very little interest!

Rescompany Systems Australia, the Macquarie Marine Research Centre and the Macquarie University Department of Mathematics and Statistics for employing me throughout the course of my studies.

The CSIRO Marine National Facility (MNF) for its support in the form of sea time on *RV Investigator*, support personnel, scientific equipment and data management. All data and samples acquired on the voyage are made publicly available in accordance with MNF Policy.

This Project is supported through funding from the Australian Government's Australian Antarctic Science Grant Program (AAS#4333).

This research was supported by the Australian Government through the Australian Research Council's Discovery Projects funding scheme (DP170100557). The views expressed herein are those of the authors and are not necessarily those of the Australian Government or Australian Research Council.

Abstract

Understanding past Southern Ocean climate is important for predicting future climate scenarios. Siliceous microfossil tests preserved in seafloor sediment can be used as proxies to investigate and reconstruct the timing of glacial/interglacial cycles and to estimate past sea-surface temperature. Well-preserved radiolarian tests were sampled from two 2.5 m sediment cores obtained from the continental slope of the Sabrina Coast region, East Antarctica, during *RV Investigator* voyage IN2017-V01. The radiolarian assemblages were used to verify that the microfossil record can be used as a proxy to reconstruct palaeoclimatic parameters in this region and to estimate summer sea-surface palaeotemperatures using the Imbrie-Kipp transfer function. This research demonstrates that the timing of glacial/interglacial cycles can be identified in Sabrina Coast sediment using the fossil radiolarian record. The Holocene and previous glacial period (i.e. Marine isotope stages 1 and 2) are clearly differentiated with Holocene oceanographic conditions being conducive to biosiliceous sedimentation, whilst conditions during glacial periods are not. Holocene summer sea-surface palaeotemperature estimates range between -3.26 °C and 3.26 °C. Future research will include a Ph.D. project using radiolarians from longer Sabrina Coast cores for palaeoclimate reconstruction over multiple glacial/interglacial cycles.

Contents

1. Introduction

The Southern Ocean is a key component of the global ocean circulation and climate systems. It is an important carbon dioxide (CO_2) sink, the site of the formation of Antarctic Bottom Water and changes in sea-surface temperature (SST) can influence wind circulation patterns, yet how these systems will respond to anthropogenic climate change is still uncertain (Azaneu et al., 2013; Caldeira and Duffy, 2000; Lamy et al., 2010; Le Quéré et al., 2018.). Regional reconstructions of past climate conditions are necessary to establish a baseline of 'normal' climate variance, and to anticipate how environmental systems may react to abrupt climate change (Masson-Delmotte et al., 2013). Despite the global importance of the Southern Ocean, high latitude areas, particularly in the Southern Hemisphere, are undersampled and understudied compared to other regions.

In the 2016/17 Austral summer, *RV Investigator* voyage IN2017-V01 surveyed the Sabrina Coast, East Antarctica, the marine exit point of the Totten Glacier (Armand et al., 2018). The Totten Glacier, part of the Aurora Basin catchment, covers an area of ~6000 km^2 and holds the ice equivalent of 3.5m of sea level rise. This glacier has a larger ice flux than any other in East Antarctica (Greenbaum et al., 2015; Rignot et al., 2013.). It is thought that warm, salty modified Circumpolar Deep Water is intruding onto the continental shelf and contributing to basal melting of the glacier (Greenbaum et al., 2015; Gwyther et al., 2014.). Models show that further warming of the ocean will increase the loss of grounded Totten Glacier ice (Roberts et al., 2017). Further research, including reconstructing palaeoclimatic variables for this region, e.g. ocean temperatures, water mass properties and sea-ice extent, is necessary.

1.1 Project Aims

The overarching goal of this study is to contribute to deciphering palaeoclimate systems of the Southern Ocean using fossil radiolarians from sediment deposited along the Sabrina Coast of East Antarctica. Two intertwined research aims will help achieve this goal:

1. Test the effectiveness of radiolarians in reconstructing ocean conditions during Quaternary glacial/interglacial cycles.

The first aim was to evaluate the effectiveness of total radiolarian abundance as a proxy to identify past glacial/interglacial cycles in the Sabrina Coast region. Where total abundance was high, radiolarian assemblages, and key taxa, were used to construct an age model and to infer the nature of the water column during the glacial/interglacial transition period and throughout the Holocene.

2. Generate radiolarian-based palaeotemperature estimates for the Holocene.

The second aim was to reconstruct sea-surface palaeotemperature using radiolarian assemblage data via the Imbrie-Kipp transfer function method.

Radiolarians are unicellular, eukaryotic marine microzooplankton typically ranging in size from 30 – 300 µm (Krabberød et al., 2011). They inhabit all parts of the World Ocean, which can be subdivided into six radiolarian biogeographic domains. The Southern Polar domain has the lowest mean annual temperature and oxygen concentration, but the highest concentrations of nutrients (i.e. silicate, nitrate and phosphate) (Boltovskoy and Correa, 2016). On a global scale, temperature is the environmental variable that best correlates with partitioning of radiolarian biogeographic domains, followed by nutrient levels and chlorophyll *a* (Boltovskoy and Correa, 2016). In polar regions, seasonal sea-ice coverage also controls radiolarian abundance with ~90% of radiolarian production occurring during summer months (Abelmann, 1999). Radiolarians are found throughout the water column and are most abundant between 100-400m (~160-550 individuals/m^3) south of 45°S.

Belonging to the supergroup Rhizaria, Radiolaria consists of 600-800 extant species in five orders: Acantharia, Collodaria, Taxopodia and the siliceous polycystine orders Nassellaria and Spumellaria (Suzuki and Aita, 2011; Suzuki and Not, 2015). Radiolarians belonging to the polycystine orders are the most commonly found in sediments and are therefore the focus of this thesis – from here on the term ‘radiolarian’ refers to polycystine radiolarians only.

Nassellaria

Nassellarians have heteropolar, somewhat conical skeletons (known as tests) that possess bilateral symmetry (Fig. 1). They are made up of one or more segments known as the cephalis, thorax, abdomen and post-abdominal segments. Seven extant superfamilies make up the Nassellaria order, these are further divided into ~25 families, ~140 genera and ~430 species (Lazarus et al., 2015; Suzuki and Aita, 2011; Suzuki and Not, 2015).

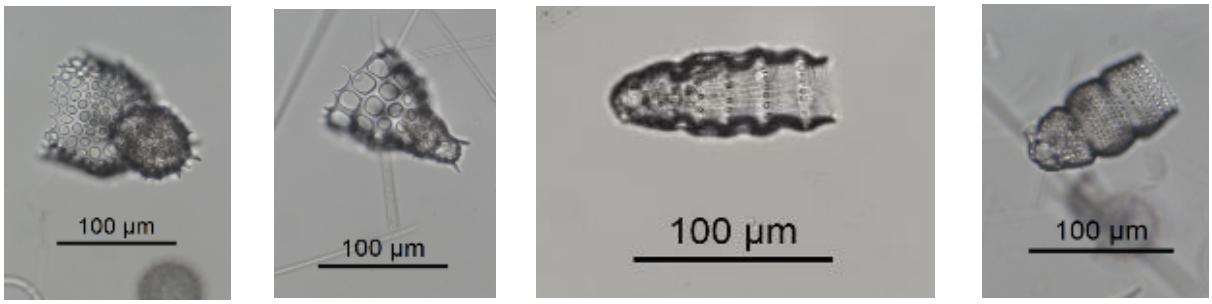

Figure 1: Nassellarian tests from Sabrina Coast sediments. Left to right: *Antarctissa* sp. (*A. strelkovi* morphotype), *Cycladophora davisiana davisiana*, *Siphocampe arachnea* and *Botryostrobus auritus-australis.*

Spumellaria

Spumellarians have tests that are spherical, elliptical, cruciate or disc shaped with shells that are spirally arranged, or concentric and connected by radial spines (Fig. 2). Radial spines can extend beyond, and additional by-spines may also be located on, the outer shell. Classification of spumellarians to genus or species level often relies on being able to view the internal skeletal structure. Nine extant superfamilies make up the Spumellaria order, and are further divided into ~30 families, ~110 genera and ~380 species (Lazarus et al., 2015; Suzuki and Aita, 2011; Suzuki and Not, 2015).

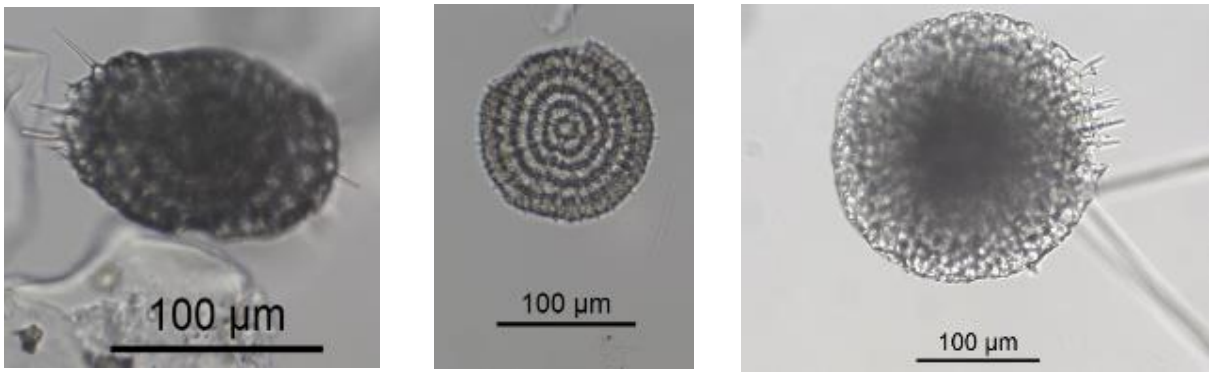

Figure 2: Spumellarian tests from Sabrina Coast sediments. Left to right: *Larcopyle weddellium*, *Stylodictya aculeata/validispina*, *Spongopyle osculosa/resurgens*.

After death, radiolarian tests sink to the ocean floor to be preserved as part of the sedimentary record. While fossil radiolarians first appeared in the Cambrian, they did not become an important part of the marine silica cycle until the Ordovician (Knoll and Kotrc, 2015). It appears only a few percent, or less, of the total assemblage is preserved in sediment, with spumellarians generally having higher preservation rates than nassellarians (Takahashi, 1991). The proportion of radiolarians preserved at individual sites is thought to be, at least in part, due to overall sedimentation rates (Takahashi, 1991). The fossil radiolarian record can be observed in, and data recorded from, sediment cores extracted from the seafloor. These data are useful in fields such as biostratigraphy, structural engineering, petroleum exploration, palaeoceanography, and in the reconstruction of

palaeoclimatic parameters such as sea-surface temperature (Knoll and Kotrc, 2015; Saraswati and Srinivasan, 2016).

2. General Methods

2.1 Core sites

Sediment cores were obtained on *RV Investigator* voyage IN2017-V01, also referred to as the Sabrina Seafloor Survey, between 14th January and 5th March 2017 (Armand et al., 2018). The vessel sailed from Hobart, Australia to the Sabrina Coast region of East Antarctica where ~44,000 km^2 of seafloor bathymetry was surveyed and mapped, and a total of 106 m of sediment core was obtained. Core tops from eight of the 13 box cores and one of the six multicores obtained during the voyage, as well as the entire length of two 250 cm box cores, are used in this project (Table 1).

Table 1: Coordinates and water depth for cores collected on IN2017-V01 and sampled for this project (Armand et al., 2018).

Core	Latitude	Longitude	Depth (m)
KC03	-64.46	115.04	1862
KC04	-64.68	119.30	3103
KC05*	-64.65	119.02	3198
KC06	-64.73	118.70	3320
KC07	-64.40	118.50	3282
KC08	-64.79	119.74	3354
KC11*	-65.13	120.05	2612
KC13	-64.48	119.10	3321
MC01	-64.47	115.62	2161

* denotes cores of which the entire length was used in this study

The two box core sites were in Area C of the IN2017-V01 survey which was dominated by four submarine canyon systems separated by asymmetric ridges (Fig. 3). The core sites were chosen where sub-bottom profiling suggested good penetration potential and stratigraphic layering. Core KC05 was taken from the lower, western side of a ridge at a depth of 3198 m. It was thought to be a low energy site with a high rate of deposition. In contrast, KC11 was taken from a ridgetop between two braided submarine canyons. It was the southernmost core obtained during the voyage and the site was selected in part due to the shallow water depth (2612 m) relative to the cores taken until that point in the voyage (Armand et al., 2018).

2.2 Sample collection and processing

KC05 and KC11 were both 250 cm long and were sampled for radiolarians at ~5 cm intervals from 0-100 cm, and ~10 cm intervals between 100-250 cm (n=36 for both cores, including core tops). Core top samples were taken from six additional box cores and one multicore also collected during the voyage. Samples were air dried at Macquarie University, at ambient temperature (~21 °C), and their processing in preparation for microscopy was based on the method of Cortese and Prebble (2015).

For each sample, 4 g of dry sediment was weighed in a 250 mL glass beaker. The MC01 core top sample is the exception as only 1.7 g of dry sediment was available. Reverse osmosis (RO) water was added to the beaker until the sediment was submerged. A similar amount of 5% Calgon (sodium hexametaphosphate) solution was added to aid in the break-up of sediment. The beaker was left to sit for 20 minutes before being placed on a hotplate set to ~100 °C. Approximately 10 mL of hydrogen peroxide (H_2O_2 - 35%) was added to the beaker to break down organic matter. Once the H_2O_2 reaction had ceased, a similar amount of hydrochloric acid (HCl - 10%) was added to break down carbonates. In both cases, more H_2O_2 or HCl was added until all organics and carbonates were removed. Once the reactions were complete (as indicated by the contents turning yellow), the contents of the beaker were left to cool before being thoroughly washed with RO water through a 45 µm sieve. The predominately siliceous residue which remained in the sieve was transferred for storage to 60 mL Nalgene bottles containing 50 mL RO water. Between each sample, the sieve was rinsed thoroughly with tap water, placed in a Soniclean containing RO water for 5 minutes, and rinsed thoroughly with RO water again.

2.3 Slide preparation and microscopy

Two sets of slides were prepared - quantitative slides (Q-slides) and counting slides (C-slides). Q-slides were made using a known quantity of suspended residue to determine the total radiolarian abundance (TA) per gram of sediment. C-slides were made using enough residue, based on the Q-slide counts, so >400 individuals could be identified and counted. C-slide counts were used to calculate relative radiolarian abundance (RA).

2.3.1 Q-slides

Q-slides were made by placing 22x22 mm coverslips on a hot plate set to ~80 °C. The Nalgene sample bottles were inverted, and a pipette used to transfer 0.8 mL RO water, then 0.2 mL aliquot, on to the coverslip. Once the water had evaporated, leaving only residue,

slides were fixed to the coverslips using Canada Balsam, inverted and left on the hotplate for at least 10 minutes to harden.

An Olympus BH-2 inverted light microscope was used to view Q-slides at 100x magnification. Samples that were very abundant in siliceous material, and therefore difficult to count, had alternative Q-slides made with 0.9 mL RO water/0.1 mL aliquot (or in one case, 0.95/0.05 mL) for ease of counting. Only radiolarian tests which were >50% complete were counted to avoid counting the same individual twice.

TA for each sample was calculated using the formula $\frac{R_T}{W_D} \times \frac{V_T}{V_A}$ where R_T = total number of radiolarians on the slide, W_D = dry weight of sediment (usually ~4g), V_T = total volume of the suspended solution (50 mL) and V_A = amount of aliquot on slide (usually 0.2 mL).

2.3.2 C-slides

C-slides were made using a similar method to Q-slides. Based on the radiolarian count of the corresponding Q-slide, aliquot estimated to contain >400 radiolarian tests was transferred to a 20x32 mm, or 20x50 mm coverslip. Initially, C-slides were not made for samples that contained fewer than 3000 tests /g due to the likelihood that the slides would not contain >400 individuals. C-slides were eventually made for some of the less abundant samples (sometimes several per sample) with varying levels of success in counting. C-slides were viewed using the same microscope as the Q-slides, this time under 200x magnification to aid with identification. An average of 493 tests per C-slide were identified, to species/subspecies or genus level where possible, and their counts recorded in the counting dataset.

Percentage RA of each taxon, for each sample, was calculated by $\frac{R_S}{R_T} \times 100$ where R_S = number of radiolarians of a particular taxon and R_T = total number of radiolarians counted.

2.4 Identification and Taxonomy

Taxonomic identification of individuals was undertaken to species/subspecies or genus level. On average 62.5% of specimens were identified to species/subspecies, 32.3% of specimens were identified to genus. Approximately half of the individuals identified to genus level were *Antarctissa denticulata* or *Antarctissa strelkovi*, which were recorded as *Antarctissa* spp. when species determination was difficult. A small proportion (average 5.2% per slide) was identified simply as belonging to either the Nassellaria or Spumellaria orders when more precise identification was not possible.

Taxonomic nomenclature used while preparing the counting dataset was per Lazarus et al. (2015) with additional clarification sought from the World Register of Marine Species (WoRMS Editorial Board, 2018) and radiolaria.org (radiolaria.org, 2018) when necessary. A table of references for the 119 species and genera identified is provided in Supplement A. Some taxa were grouped to align with the modern analogue dataset by Cortese and Prebble (2015) (Table 2). Some genera, as well as the individuals identified only as Nassellaria or Spumellaria, were removed due to taxonomic uncertainty. Statistical analyses were performed on the counting dataset after taxonomic standardisation. The standardised analysis dataset contained 76.8% of the individuals recorded in the raw counting dataset. An average of 378 individuals per sample were included in the analysis dataset.

Table 2: Radiolarian taxa grouped prior to analyses.

Actinomma delicatulum/popofskii
- *Actinomma delicatulum*
- *Actinomma popofskii*

***Actinomma leptodermum* s.l.**
- *Actinomma leptodermum*
- *Actinomma lepto longispina*

***Antarctissa* spp.**
- *Antarctissa* spp.
- *Antarctissa cylindrica*
- *Antarctissa denticulata*
- *Antarctissa strelkovi*

***Cenosphaera* spp.**
- *Cenosphaera cristata*
- *Cenosphaera* spp.

Dictyophimus crisiae/hirundo
- *Dictyophimus crisiae*
- *Dictyophimus hirundo*

Druppatractus variabilis/ostracion
- *Druppatractus ostracion*
- *Druppatractus variabilis*

***Eucyrtidium* spp.**
- *Eucyrtidium* spp.
- *Eucyrtidium annulatum*
- *Eucyrtidium teuscheri*

***Lithomelissa boreale* gr.**
- *Lithomelissa boreale*
- *Lithomelissa hystrix*
- *Trisulcus testudus*

***Phormacantha* spp.**
- *Phormacantha* spp.
- *Phormacantha hystrix*

***Pseudodictyophimus gracilipes* s.l.**
- *Pseudodictyophimus bicornis*
- *Pseudodictyophimus gracilipes*
- *Pseudodictyophimus multispinus*

Saccospyris antarctica
- *Botryocampe conithorax*
- *Saccospyris* spp.
- *Saccospyris antarctica*
- *Saccospyris conithorax*

Spongopyle osculosa/resurgens
- *Spongodiscus resurgens*
- *Spongopyle osculosa*

Stylodictya aculeata/validispina
- *Stylodictya aculeata*
- *Stylodictya validispina*

3. Radiolarians as indicators of Quaternary glacial/interglacial cycles

3.1 Introduction

The first aim of this thesis was to establish if radiolarian assemblages in Sabrina Coast sediments are useful as proxies to identify large-scale Quaternary palaeoclimate events/trends. Since well before the Quaternary (2.58Ma – present), Earth's climate has been dominated by glacial/interglacial cycles of varying lengths, dictated by variances in orbital eccentricity, obliquity and precession, each with varying degrees of influence (Lisiecki and Raymo, 2005). Since Marine Isotope Stage (MIS) 22 (~0.88 – 0.87 Ma) the pace of these cycles has been set by ~100 ka cycles of orbital eccentricity. Glacial periods are characterised by prolonged glaciation and extensive sea-ice coverage at mid- and high-latitudes as well as high altitudes. Throughout the Holocene (11.7 ka - present) Earth has experienced interglacial conditions where year-round glaciation or sea-ice coverage is restricted to polar and/or high-altitude regions. In this chapter, radiolarian TA was evaluated as a potential indicator of glacial/interglacial conditions in the Sabrina Coast region of Antarctica. For periods where TA was high enough to derive assemblage data, radiolarian assemblage composition and key species were used to infer oceanic conditions. For example, knowledge of the environmental preferences of *Cycladophora davisiana davisiana* (henceforth simply *C. davisiana,* Fig. 1) can be used as a stratigraphic tool in palaeoclimate reconstructions. High *C. davisiana* abundances are a known marker of glacial/interglacial transition periods. Variation in the abundance of *C. davisiana* in Pleistocene sediments was a key piece of evidence in verifying that orbital Milankovitch cycles were related to the timing of Pleistocene glaciations (Hays et al., 1976).

3.2 Methods

3.2.1 Complementary datasets

Independent data from IN2017-V01, and used in conjunction with radiolarian TA, is described below.

Magnetic susceptibility

The magnetic susceptibility (MS; unit = k) of KC05 and KC11 was measured onboard during IN2017-V01. MS is a dimensionless measure of the magnetic properties of a material and, when used in the context of deep-sea sediment cores, can highlight changes in the composition of seafloor sediments, and can be used for core to core correlation within a

region (Richter et al., 2007). Low MS values may indicate a high proportion of biogenic to terrigenous material, while high MS values may indicate the opposite.

Geochronology

Carbon-14 (^{14}C) dates were determined for two depths in KC05 where sufficient foraminifera specimens were present. Foraminifera are single-celled eukaryotic organisms with some species making calcium carbonate ($CaCO_3$) tests. The carbon from their tests can be dated using ^{14}C methods (Dowsett, 2009). Due to the very low abundance of foraminifera in KC05, as typical for very high latitude sites, only two samples contained enough foraminifera to calculate ^{14}C based dates. The 220 cm layer yielded a date of 33.77 ka (+/- 0.35 ka), while a sample from the core catcher (i.e. at a greater depth than 250 cm) was dated at 45.96 ka (+/- 2.4 ka) (Perera, 2017) No ^{14}C dating is yet available for KC11.

Diatom abundance

Diatom TA was calculated for KC05 and KC11 using similar methods to radiolarian TA. Diatoms are siliceous, unicellular algae, found in both freshwater and marine environments, and can be planktonic, free-floating or attached to the substrate (Leventer, 2009). In the Southern Ocean, diatom distribution is typically related to sea ice and SST which makes them an ideal proxy for reconstructing palaeoclimate parameters (Armand et al., 2005; Zielinski and Gersonde, 1997). Quantitative slides for diatom work were prepared and counted at the Micropaleontology Lab, Geology Department, Colgate University, by Isabel Dove and Meaghan Kendall.

3.2.2 Diversity Indices

Where radiolarian TA was sufficient, raw count data was used to calculate several diversity indices:

- Taxon richness (S) i.e. the number of taxa per sample,
- Shannon's diversity index (H), a measure which considers both abundance and evenness of taxa, was calculated in R using the *diversity* function in the *vegan* package (Oksanen et al., 2018),
- Evenness (E_H) of taxa was derived from H using the formula $E_{H\,i} = \frac{H_i}{ln(S_i)}$,
- Chao-1, an estimate of true taxon richness based on sample counts, was generated using the computer package Paleontological Statistics 3.16 (PAST) (Hammer, Harper, and Ryan, 2001), and

- The ratio of Nassellaria to Spumellaria taxa (RNS) was calculated using the formula $RNS = \frac{RA_{Nass}}{RA_{Nass}+RA_{Spum}}$.

For correlations involving core depth as a proxy for time, Spearman's rho (rho) and associated *p*-value were used to relax the assumption of a constant sedimentation rate. For correlations with radiolarian TA, Pearson's (r) and associated *p*-value were used. Pearson and Spearman correlations were calculated using the *cor.test* function in R (R Core Team, 2018).

3.2.3 Cluster Analysis

Cluster analysis is a multivariate tool used to classify variables into groups based on the similarity of the observations within each variable (van Tongeren, 1995). In this case, the similarities between the radiolarian assemblage of each sample were used to group the samples. The R functions *hclust* (R Core Team, 2018) and *dendextend* (Galili, 2015) were used to perform hierarchical cluster analysis with the Bray-Curtis similarity measure and complete (i.e. furthest neighbour) linkage. Using the Jaccard similarity measure resulted in the same clustering as Bray-Curtis. After clusters were identified, One-way Analysis of Similarities (ANOSIM) was conducted using PAST (Hammer et al., 2001) to determine if there was a significant difference between two or more of the clusters. The average RA of the top ten most abundant species (based on the overall RA of each species) was calculated and One-way Analysis of Variance (ANOVA) was run using PAST (Hammer et al., 2001) to see which of these ten species had a significantly different average RA per cluster. For species where the equal variances assumption was not satisfied (*Botryostrobus auritus-australis*, *Larcopyle weddellium* and *Siphocampe arachnea*) Welch's test was used.

3.3 Results

3.3.1 Total radiolarian abundance

Core tops

Radiolarian TA in Sabrina Coast core tops ranged from ~400 tests /g (KC07) to >40,000 tests /g (KC03) (Fig. 3). Neither latitude nor longitude appeared to influence radiolarian core top TA (r = -0.05, *p* = 0.91; r = -0.52, *p* = 0.15 respectively), however, higher radiolarian TA was observed in the shallower parts of the region (r = -0.7, *p* = 0.03).

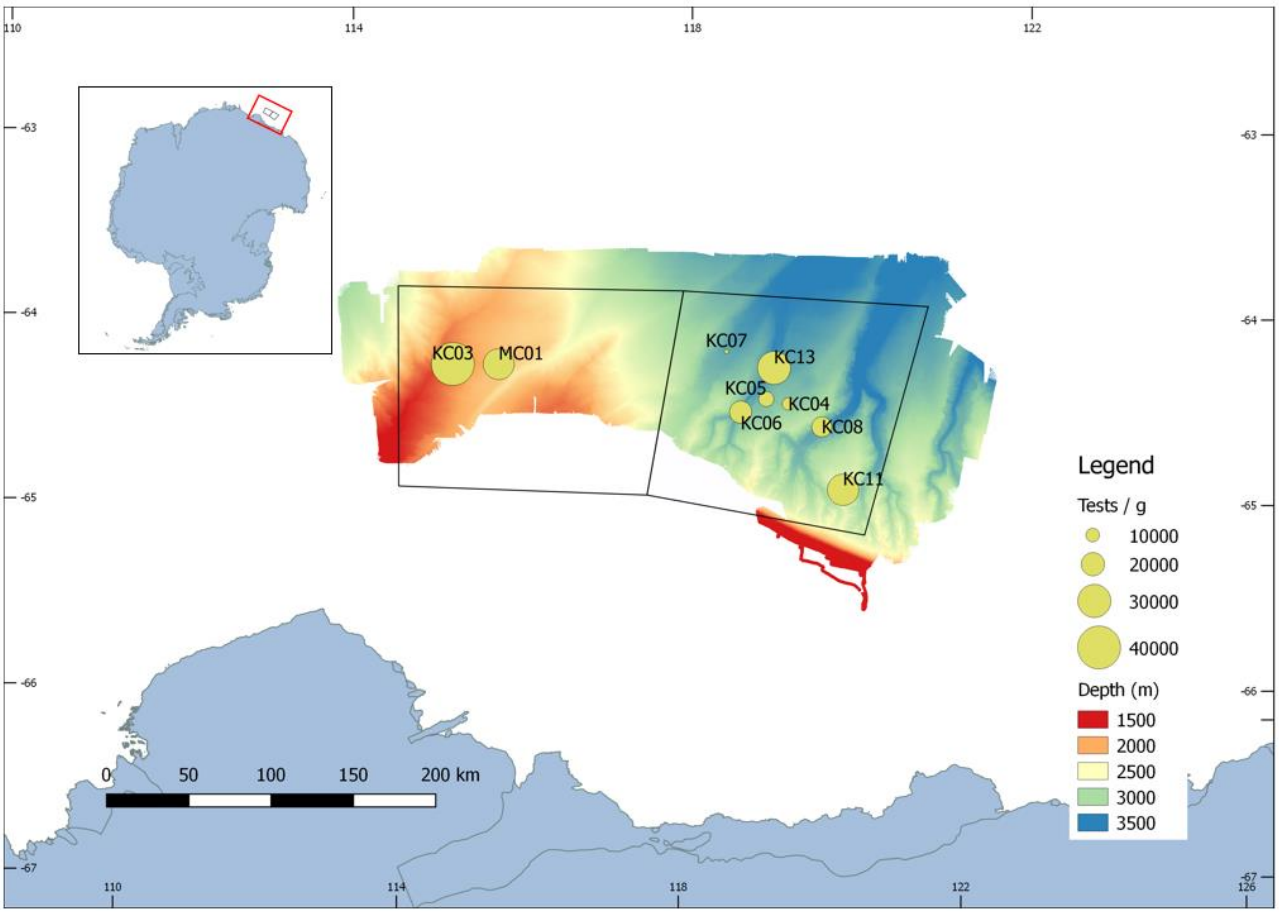

Figure 3: Total radiolarian abundance (TA) for Sabrina Coast core tops. There is evidence that core tops from shallower water depths tend to have higher radiolarian TA (r = -0.7, *p* = 0.03).

KC05

Radiolarian TA peaked at 26 cm (~62 x 10^3 tests /g), peak diatom TA occurred at a similar depth (37 cm, ~163 x 10^6 valves /g) and most samples below 66 cm contained virtually no biosiliceous microfossils (Fig. 4). MS was relatively low until ~40 cm indicating a higher than normal ratio of biosiliceous to terrigenous sediment, and, beyond this, quite variable. Towards the lower part of the core, both radiolarian and diatom TA increased slightly at ~200-210 cm. Radiolarian and diatom TA follow a similar pattern (r = 0.852, $p < 0.001$), and radiolarian TA is significantly negatively correlated with MS (r = -0.714, $p < 0.001$), throughout the core. Carbon-14 dating indicates that the age of the core at 220 cm is ~33.8 ka. This may place the small peak in radiolarian and diatom TA at 209cm around the time of the MIS 3/2 boundary (~29 ka, Lisiecki and Raymo, 2005).

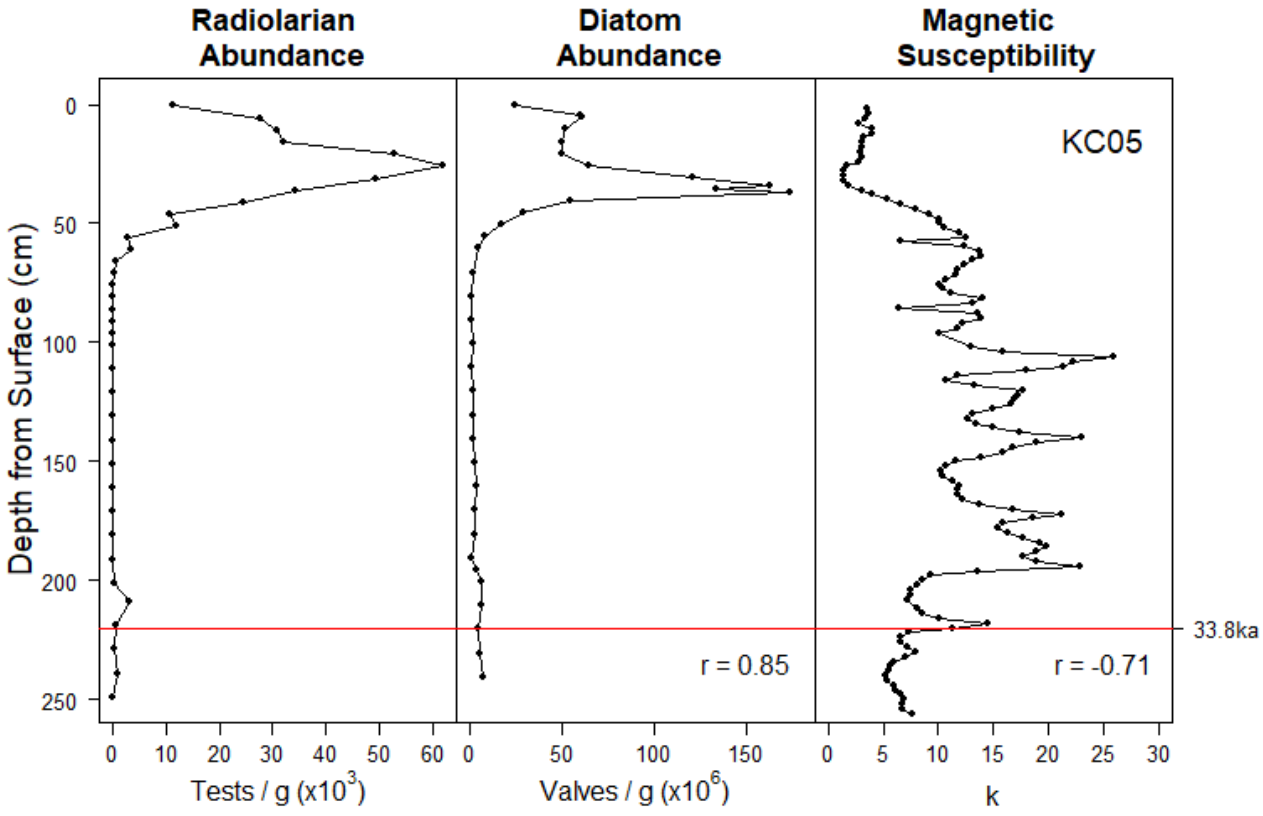

Figure 4: Radiolarian and diatom total abundance (TA), and magnetic susceptibility for KC05. Pearson's r values show the correlation between the plotted parameter and TA, both are statistically significant with $p < 0.001$. Radiolarian and diatom abundance fall dramatically at ~50 cm (between 18.5 and 10.2 ka see section 3.4.4). Horizontal line at 220 cm indicates a foraminifera-derived ^{14}C age of 33.8 ka (Perera, 2017).

KC11

Radiolarian TA peaked at 38 cm (~48 x 10^3 tests /g) and diatom TA peaked at 55.5 cm (~99 x 10^6 valves /g) (Fig. 5). Both radiolarian and diatom TA dropped at ~100 cm with small peaks at ~120 cm (~11 x 10^3 tests /g, ~ 41 x 10^6 valves /g respectively). Samples below 138 cm contained virtually no biosiliceous microfossils. MS was relatively low until ~80 cm and, beyond this, quite variable. Radiolarian and diatom TA curves are similar (r = 0.89, $p < 0.001$) and radiolarian TA is significantly negatively correlated with MS (r = -0.9, $p < 0.001$) throughout the core. These results are consistent with those seen in KC05.

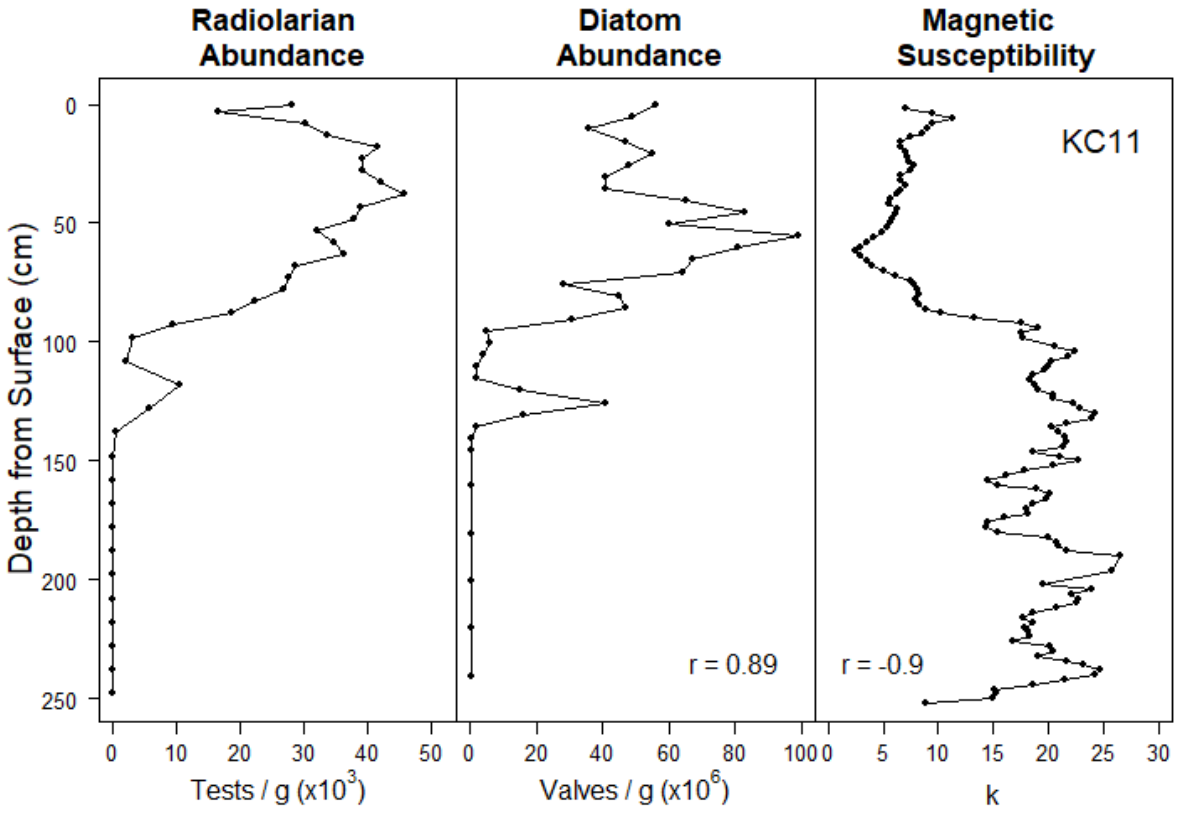

Figure 5: Radiolarian and diatom total abundance (TA), and magnetic susceptibility for KC11. Pearson's r values show the correlation between the plotted parameter and radiolarian TA, both are statistically significant with $p < 0.001$.

3.3.2 Diversity Indices

Diversity indices were calculated for the radiolarian-rich, upper portions of KC05 (0-66 cm) and KC11 (0-138 cm). The final analysis included the core tops (excluding KC07 due to its low TA), upper portions of both cores (i.e. 0-66cm for KC05 and 0-138cm for KC11) and sample KC05-209. The other samples did not have a high enough TA to derive assemblage data and will be excluded from further analyses.

KC05

Radiolarian taxon richness in KC05 samples ranged from 35 taxa (66 cm) to 52 taxa (31 cm), Shannon's H ranged from 2.54 (66 cm) to 3.03 (0 cm), evenness ranged from 0.70 (16 cm) to 0.79 (0 cm), Chao-1 species richness measure ranged from 39 (66 cm) to 61.11 (26 cm) and RNS ranged from 0.74 (6 cm) to 0.84 (26 cm) (Fig. 6). Of these indices, taxon richness (rho = -0.56, p = 0.04) and Shannon's H (rho = -0.56, p = 0.04) decreased significantly with depth. Taxon richness (r = 0.62, p = 0.02), Chao-1 (r = 0.64, p = 0.01) and RNS (r = 0.67, p = 0.01) were positively correlated with radiolarian TA despite being

independently quantified. Depth and TA are also negatively correlated (rho = -0.58, *p* = 0.03).

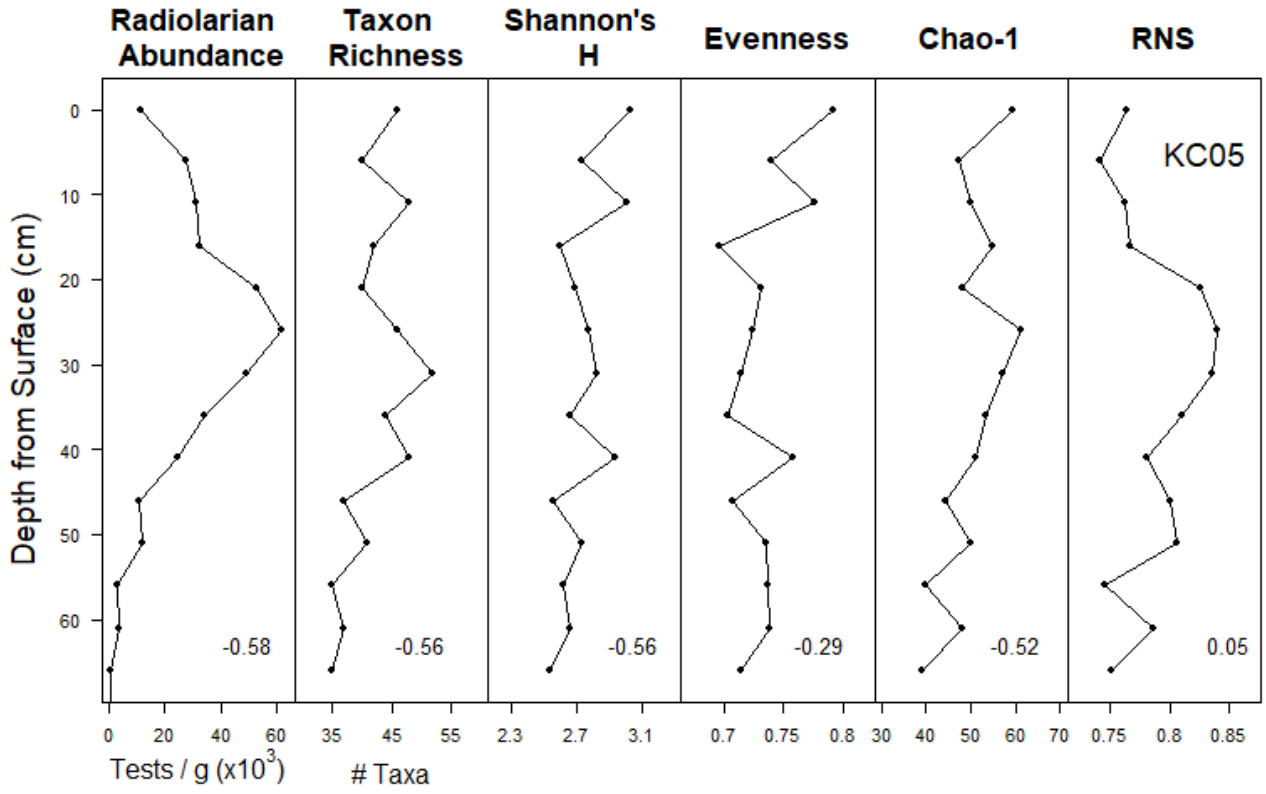

Figure 6: Radiolarian total abundance, taxon richness, Shannon's H index, evenness, Chao-1 and RNS values for KC05. Spearman's rho values show the correlation between the plotted parameter and depth. Statistically significant correlations with depth are total abundance (rho = -0.58, *p* = 0.03), taxon richness (rho = -0.56, *p* = 0.04) and Shannon's H (rho =-0.56, *p* = 0.04).

KC11

Radiolarian taxon richness in KC11 samples ranged from 38 taxa (78 cm and 138 cm) to 61 taxa (3 cm), Shannon's H ranged from 2.55 (108 cm) to 3.32 (3 cm), evenness ranged from 0.69 (98 cm) to 0.82 (13 cm), Chao-1 species richness measure ranged from 44 (138 cm) to 109 (33 cm) and RNS ranged from 0.70 (138 cm) to 0.89 (63 cm) (Fig. 7). Of these indices, Shannon's H (rho = -0.49, *p* = 0.01) and evenness (rho = -0.45, *p* = 0.02) decreased significantly with depth. RNS (r = 0.41, *p* = 0.04) was positively correlated with radiolarian TA. Depth and TA are significantly negatively correlated (rho = -0.69, *p* < 0.001).

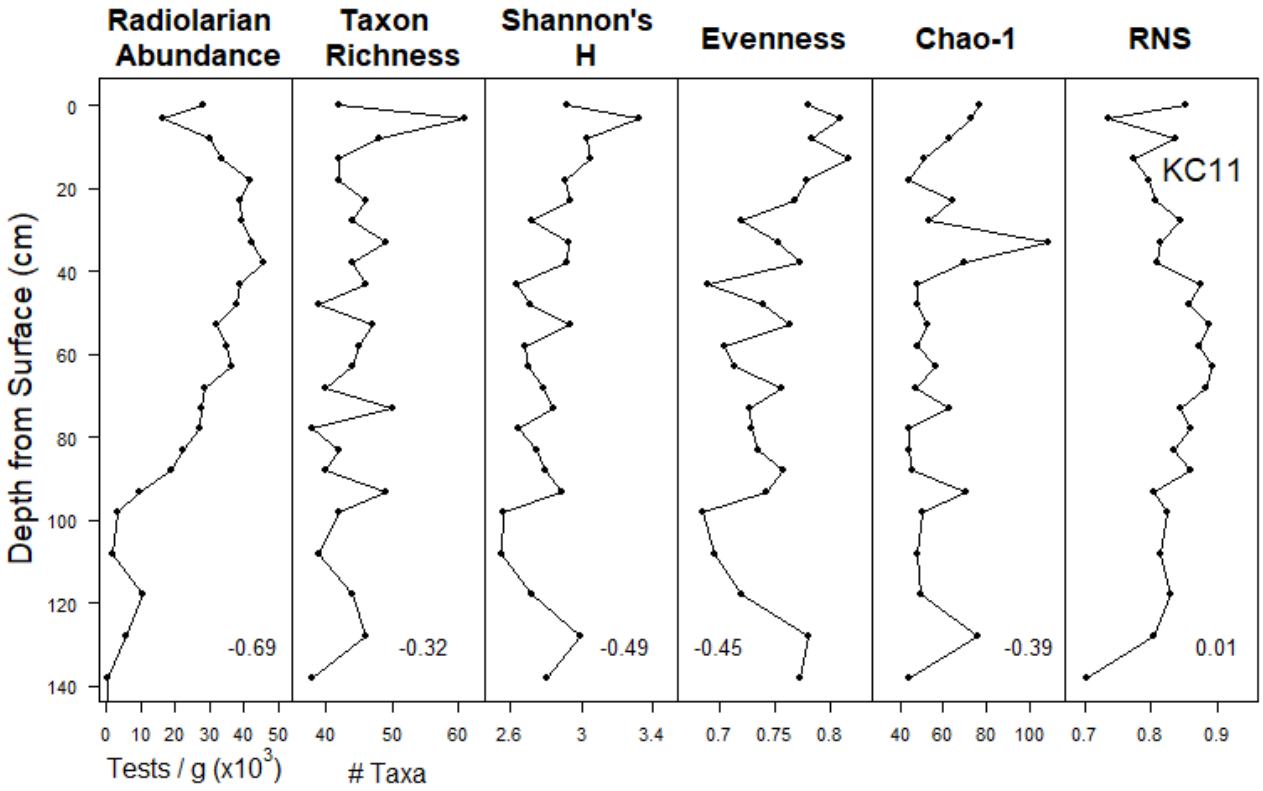

Figure 7: Radiolarian total abundance, taxon richness, Shannon's H index, evenness, Chao-1 and RNS values for KC11. Spearman's rho values show the correlation between the plotted parameter and depth. Statistically significant correlations with depth are total abundance (rho = -0.69, $p < 0.001$), Shannon's H (rho = -0.49, $p = 0.01$) and evenness (rho = -0.45, $p = 0.02$).

3.3.3 Cluster Analysis

Once again, only those samples for which RA data could be derived, i.e. the samples with a high enough TA, were included in the cluster analysis, this time including sample KC05-209. Using hierarchical cluster analysis, samples were classified into four clusters with this number being selected as the most appropriate (Fig. 8). Cluster 1 (n=22) consists of six core tops (all core tops excluding KC03 and KC08), and samples from the upper half of KC05 and upper third of KC11. Two samples in the bottom third of KC11 (KC11-118 and KC11-128) were also classified as belonging to Cluster 1. Cluster 2 (n=10) consists of the two remaining core tops, one sample from KC05 (KC05-31) and the middle third of KC11. Cluster 3 (n=13) consists of the lower half of KC05 and the lower third of KC11, except for the two samples which were previously classified into Cluster 1. Sample KC05-209 was identified as the lone sample in Cluster 4 and, as this sample is something of an outlier in

both its core depth and assemblage, it will not be discussed alongside the three 'main' clusters.

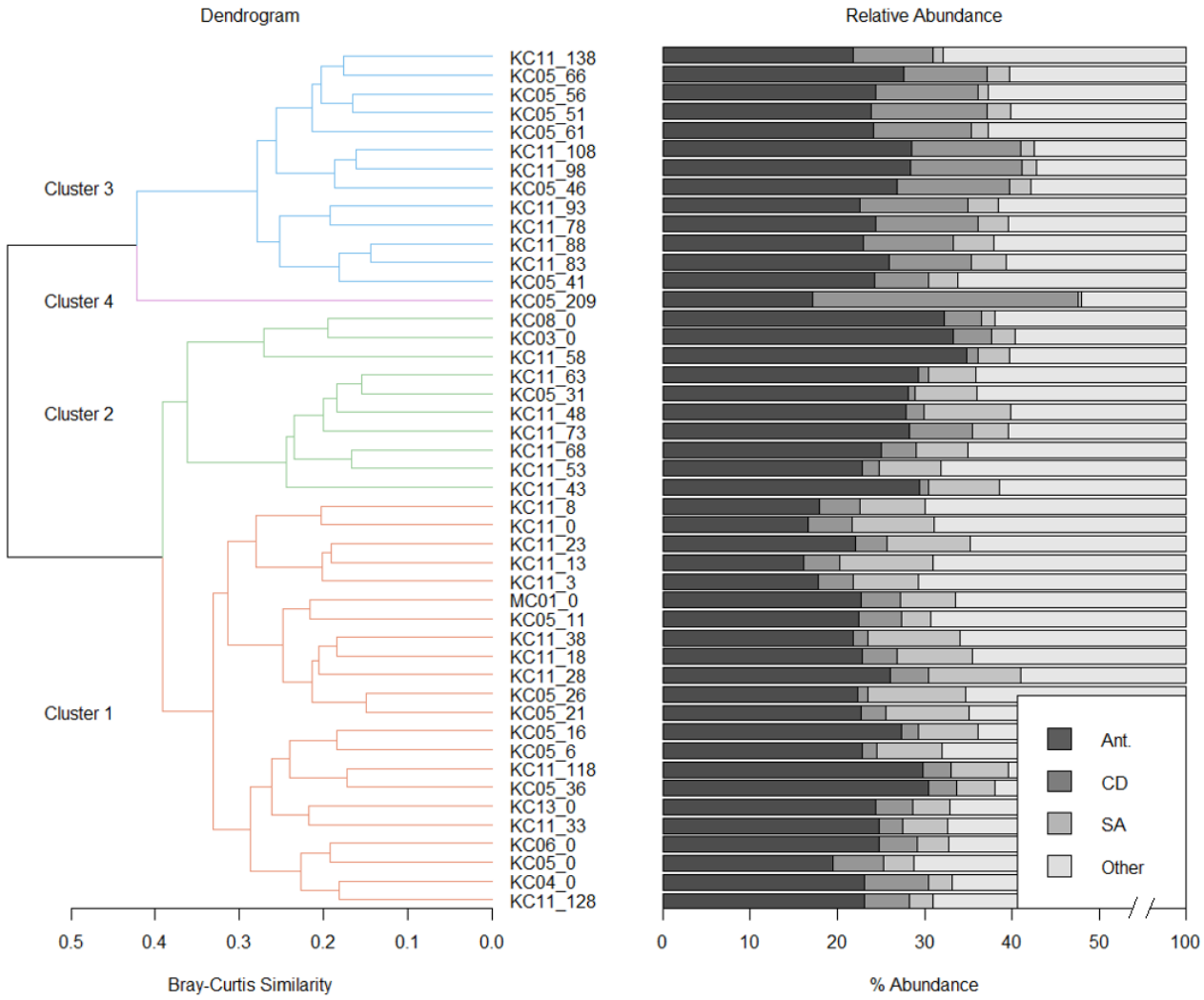

Figure 8: Dendrogram of clustered samples with stacked bars representing the accompanying relative abundance of three important radiolarian taxa, *Antarctissa* spp. (Ant.), *C. davisiana* (CD) and *S. arachnea* (SA), and one category containing all other radiolarian taxa in the assemblage. Cluster 1 had the highest average RA of *S. arachnea*, Cluster 2 had the highest average RA of *Antarctissa* spp. and Cluster 3 had the highest average RA of *C. davisiana*.

ANOVA showed a significant difference in average radiolarian TA between at least two of the clusters ($r = 0.65$, $p < 0.001$). Tukey pairwise comparison tests showed that regarding mean TA, Cluster 3 (mean TA = 10.6×10^3 tests /g) was significantly different from Clusters 1 (mean TA = 30×10^3 tests /g) and 2 (mean TA = 35.5×10^3 tests /g). ANOSIM of the three

main clusters shows that there is a significant difference in assemblage between at least two of the clusters (r = 0.62, $p < 0.001$). Clusters 2 and 3 are the most dissimilar (pairwise ANOSIM test, r = 0.75, $p < 0.001$), followed by Clusters 1 and 3 (r = 0.71, $p < 0.001$), and Clusters 1 and 2 (r = 0.42, $p < 0.001$). Canonical correspondence analysis (Supplement C) also supports the conclusion that Cluster 3 is very different from Clusters 1 and 2 with Cluster 4 being an outlier.

The per-cluster RA averages of the ten most abundant taxa were used to identify those that may best explain the differences between clusters (Table 3). ANOVA and Tukey pairwise comparison tests show six of the top ten taxa have significantly different RA in at least two of the clusters (Fig. 9). The RA of *C. davisiana* and *S. arachnea* account for the difference between Clusters 1 and 2, and Cluster 3. Clusters 1 and 2 have relatively high *S. arachnea* RA averages (6.9% and 5.5% respectively) and lower *C. davisiana* RA averages (3.8% and 2.8%). Cluster 3 has a lower *S. arachnea* average RA (2.6%) and a higher *C. davisiana* average RA (11%). Differences between Clusters 1 and 2 lie in the significantly different average RA of *Antarctissa* spp. (22.8% vs 29.1%, $p < 0.001$), *L. weddellium* (2.7% vs. 1.1%, $p < 0.001$), *Lithomelissa* sp. A (3.2% vs 5.2%, $p < 0.001$) and *S. antarctica* (1.0% vs 1.9%, $p < 0.001$). The average RA of the remaining taxa (*B. auritus-australis*, *L. platycephala*, *P. longispinum* and *P. gracilipes* s.l.) do not differ significantly between clusters.

Table 3: Average relative abundance (%) of the ten most abundant radiolarian taxa.

	Average relative abundance (%)			
Species	**Overall**	**Cluster 1**	**Cluster 2**	**Cluster 3**
Antarctissa spp.	24.68	22.79	29.12	25.05
Botryostrobus auritus-australis	1.90	1.61	2.32	2.14
Cycladophora davisiana davisiana	6.20	3.84	2.78	10.97
Larcopyle weddellium	1.92	2.66	1.08	1.33
Lithocampe platycephala	1.91	1.91	2.25	1.74
Lithomelissa sp. A	3.75	3.20	5.21	3.79
Peridium longispinum	1.64	1.87	1.99	1.12
Pseudodictyophimus gracilipes s.l.	3.89	4.20	3.84	3.43
Saccospyris antarctica	1.62	0.97	1.87	2.59
Siphocampe arachnea	5.27	6.92	5.55	2.65

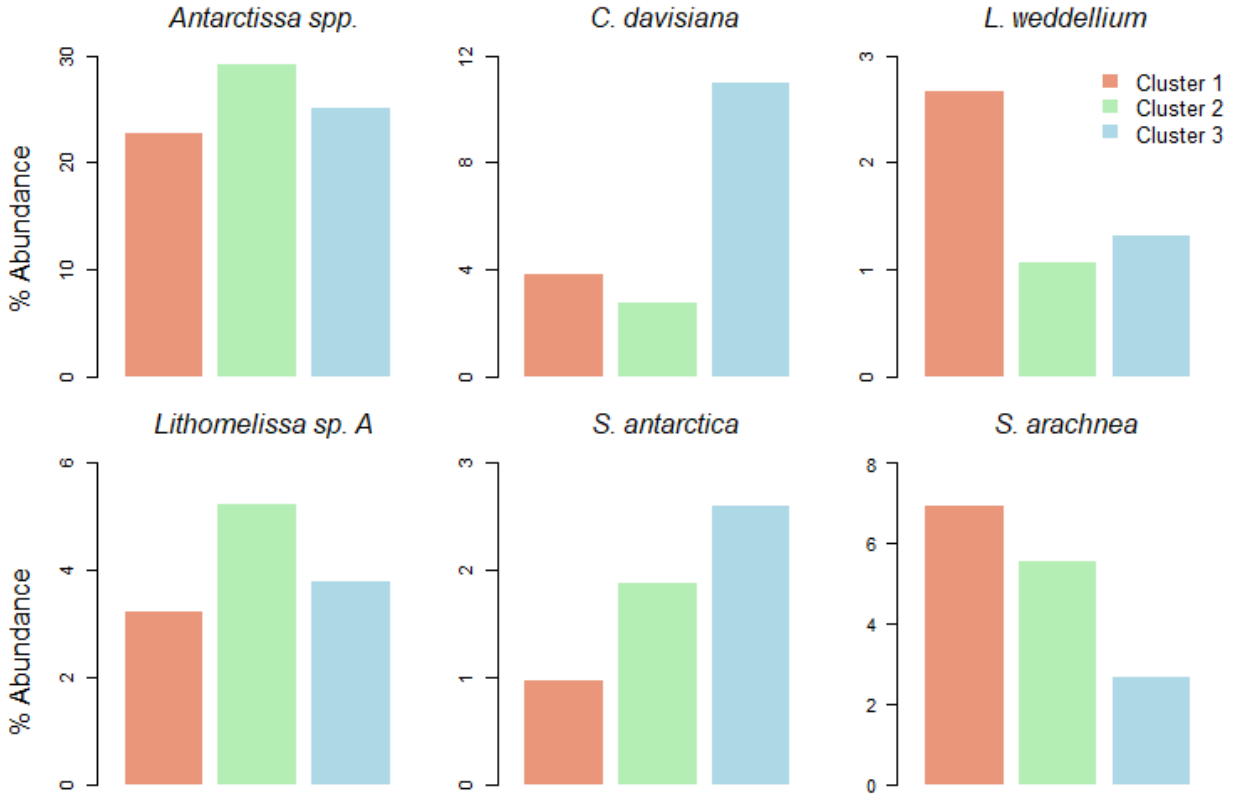

Figure 9: Average RA (% Abundance) by cluster of six taxa for which Tukey's pairwise comparison tests showed a significant difference in average relative abundance between clusters. Note that the axis representing average RA varies for each taxon presented.

The classification of sample KC05-209 into a cluster of its own can be explained by the dominance of *C. davisiana* (RA = 30.4%). In comparison, the second highest RA of *C. davisiana* is only 13.2%. KC05-209 is also the only sample in which *Antarctissa* spp. are not the most abundant. Due to the lack of viable samples either side of KC05-209, it is not possible to tell if this is an isolated incident of high *C. davisiana* abundance, relatively high radiolarian TA in general, or part of a meaningful signal which may have been observed with higher resolution sampling at this depth.

Cluster analysis, ANOSIM and canonical correspondence analysis, show the assemblages can be classified into three main clusters, with KC05-209 being the lone sample in Cluster 4. Of the three main clusters, Cluster 3 is distinct from the more similar Clusters 1 and 2 mostly due to the differences in RA of *C. davisiana* and *S. arachnea* (Fig. 10).

3.3.4 Cycladophora davisiana and Siphocampe arachnea

Cycladophora davisiana RA follows a similar pattern in both KC05 and KC11 with most upper core values being ≤5% abundance (Fig. 10) and values >10% seen in the lower part

of the radiolarian-rich section of core. *Cycladophora davisiana* RA ranged from 0.8% (31 cm) to 13.2% (51 cm) in KC05, and from 1% (43 cm) to 12.7% (98 cm) in KC11. It has a strong negative correlation with radiolarian TA in both KC05 (r = -0.84, $p < 0.001$) and KC11 (r = -0.71, $p < 0.001$), and a moderately positive correlation with depth in both KC05 (rho = 0.65, $p = 0.02$) and KC11 (rho = 0.44, $p = 0.03$).

Siphocampe arachnea RA values decrease with depth in both cores, except for a small peak in abundance at KC11-118. Its RA ranged from 1.3% (56 cm) to 11.2% (26 cm) in KC05 and from 1.1% (138 cm) to 10.7% (13 cm) in KC11. *Siphocampe arachnea* has a strong positive correlation with radiolarian TA in both KC05 (r = 0.91, $p < 0.001$) and KC11 (r = 0.74, $p < 0.001$) and a strong negative correlation with depth in both KC05 (rho = -0.66, $p = 0.01$) and KC11 (rho = -0.81, $p < 0.001$).

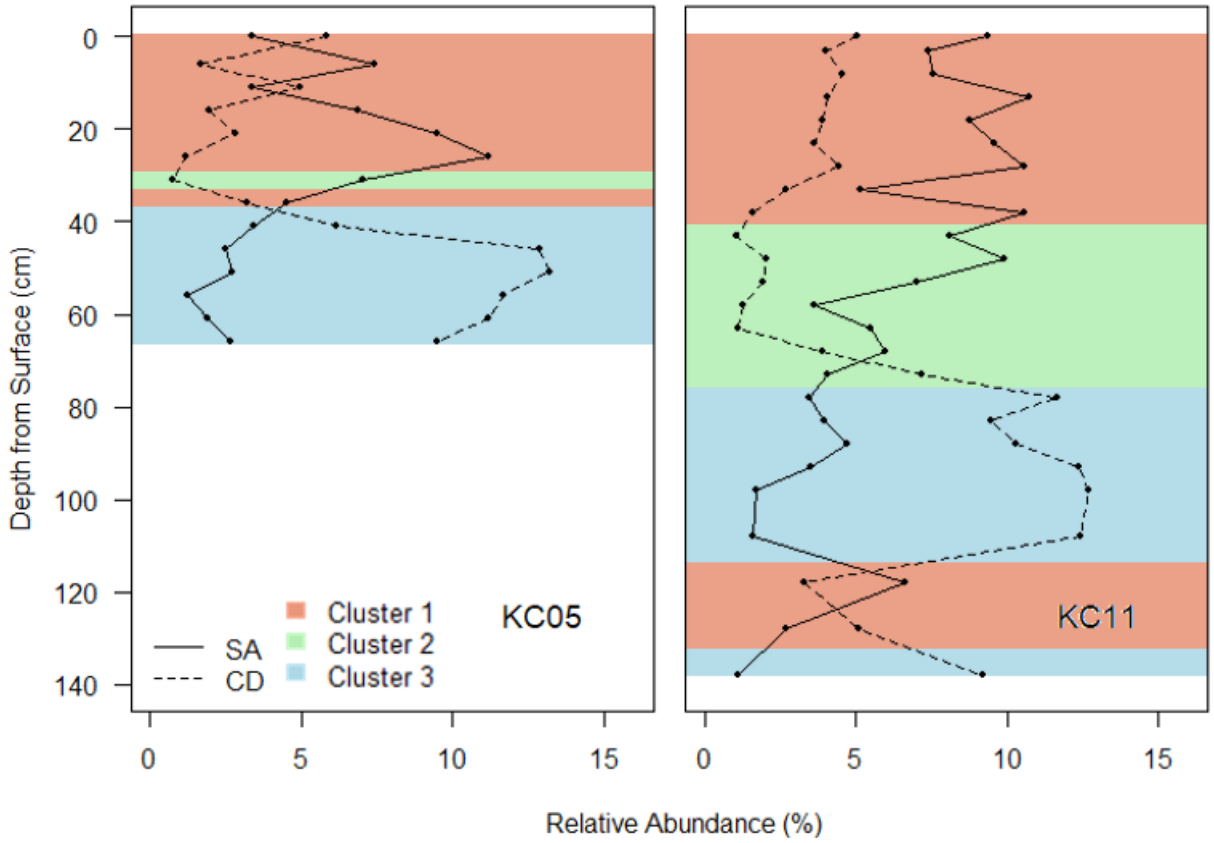

Figure 10: *Cycladophora davisiana* (CD) and *Siphocampe arachnea* (SA) relative abundance during the Holocene/Termination I. Cluster membership is overlaid (Section 3.3.3).

For ease of interpretation, the ratio of the RA of *C. davisiana* and *S. arachnea* (RCS) was calculated using the formula $RCS = \frac{RA_{Cycl}}{RA_{Cycl}+RA_{Siph}}$. RCS ranged from 0.1 (26 cm) to 0.9 (56 cm) in KC05 and from 0.11 (43 cm) to 0.9 (138 cm) in KC11. RCS was strongly positively

correlated with depth in both KC05 (rho = 0.68, p = 0.01) and in KC11 (rho = 0.58, p = 0.01), and strongly negatively correlated with TA in both KC05 (r = -0.9, p < 0.001) and KC11 (r = -0.82, p < 0.001).

3.4 Discussion

3.4.1 Key Sabrina Coast radiolarian species

Antarctissa spp. are abundant in, but not limited to, Southern Ocean waters (Boltovskoy et al., 2010) and was the dominant taxa in all radiolarian assemblages except for KC05-209. The *Antarctissa* spp. group consisted of the morphotypes *A. cylindrica*, *A. denticulata* and *A. strelkovi*. This grouping is commonly observed in radiolarian surveys (Boltovskoy et al., 2010) and aligns with the Cortese and Prebble (2015) core top dataset. In this study *A. denticulata* (most abundant between -1 and 2 °C) and *A. strelkovi* (0-5 °C) were found in significantly higher quantities than *A. cylindrica* whose distribution tends to lie in warmer waters between the Polar and Subantarctic Fronts (Abelmann et al., 1999).

Cycladophora davisiana was found in high abundances in Cluster 3 samples. *Cycladophora davisiana* is cosmopolitan and generally inhabits water depths below 200m, with living specimens being found in plankton tows of 400-1000m (Abelmann and Gowing, 1997; Matul, 2011; Morley and Hays, 1983). In addition, the calibration of absolute and relative abundance curves of *C. davisiana* with oxygen isotope curves in Quaternary sediments has enabled this species to be used as a biostratigraphic marker for age control where quantitative methods of dating are not possible (e.g., ^{14}C dates based on foraminifera tests in regions affected by carbonate dissolution) (Matsuzaki and Itaki, 2017). The current biogeographic distribution of *C. davisiana* does not appear to be correlated with SST so other factors explaining its distribution have been explored (Lozano and Hays, 1976; Petrushevskaya, 1967; both as cited in Hays et al., 1976). In the modern-day Sea of Okhotsk, near Japan, *C. davisiana* RA can reach more than 20%, whereas abundances of less than 5% are more typical elsewhere (Morley and Hays, 1979; Morley and Hays, 1983; Robertson, 1975 as cited in Hays et al. 1976). After the winter sea-ice melt, the water column in the Sea of Okhotsk is highly stratified with low-salinity surface water overlying a cold, intermediate water mass. This vertical structure can affect the distribution and abundance of surface-dwelling species while providing stable conditions for intermediate and deep-dwelling species such as *C. davisiana* (Morley and Hays, 1983). Summertime peaks in *C. davisiana* abundance in the Sea of Okhotsk suggest that its distribution may be related to these water column properties. Peaks in *C. davisiana* abundance curves (values of >5% RA

are known as Davisiana Events, or DAE's (Matsuzaki et al., 2014)) from both northern and southern high latitude Pleistocene sediments have been shown to coincide with sea ice fluctuations associated with the transition between glacial and interglacial periods (Matsuzaki et al., 2014; Matul, 2011).

Siphocampe arachnea RA was highest in Clusters 1 and 2 and is strongly negatively correlated with *C. davisiana* abundance. *Siphocampe arachnea* is a cosmopolitan species abundant at relatively shallow depths (100-300m) at both poles and found at greater depths (300-1000m) in mid-latitude waters (Boltovskoy, 1994; Boltovskoy and Correa, 2016). The negative correlation of *S. arachnea* with *C. davisiana* in Sabrina Coast sediments, and the importance it has in determining cluster membership, means research efforts should focus on this somewhat less studied species (in comparison to *Antarctissa* spp. and *C. davisiana*).

3.4.2 Glacial/interglacial radiolarian patterns

Radiolarian TA abundance varies throughout the length of the core. Radiolarian-rich sediment appearing in the more recent part of the core has been interpreted as being the current interglacial, while the absence of radiolarian tests further down core is interpreted as being an indicator of prolonged periods of sea ice cover throughout the last glacial period. This aligns with the finding that the survey area was covered by year-round sea ice at the time of the last glacial maximum (Gersonde et al., 2005). Within the radiolarian-rich sections of core, the taxon composition differs enough over time for two main stages to be identified. The transition period between the glacial/interglacial conditions of MIS 2 and 1 (also known as "glacial termination I", or "Termination I" in short) is distinguished by the high RA of *C. davisiana*, a known marker of glacial/interglacial transition periods (Matsuzaki et al., 2014). During this transition period there may have been significant stratification in the water column, similar to that seen during the summer in the modern-day Sea of Okhotsk, with a low salinity surface layer capping a cool, stable intermediate water layer (Morley and Hays, 1983). Samples which have high *C. davisiana* RA were grouped together in Cluster 3 and all occur in the lower part of the radiolarian-rich section of core. After this transition period, *C. davisiana* RA decreases and *S. arachnea* RA increases. The difference in the RA of these two species is the main factor in dividing the radiolarian-rich section of core into its two stages. Once well into the interglacial, the region was likely to have been sea-ice free for large parts of the year with summer conditions suitable for high abundances of both radiolarians and diatoms. The abundance of *S. arachnea* in mid-late Holocene sediments may be a sign of deep-water upwelling and mixing with the surface water, marking the end of the stratification seen during Termination I (Fig. 11).

Variations in radiolarian TA and composition, as well as the excellent preservation seen in these cores, means further research should incorporate the use of radiolarians in Sabrina Coast palaeoclimate reconstructions. Radiolarians have been shown to provide information on the vertical structure of the water column and the presence/absence of sea ice during critical climate transitions and intervals.

3.4.3 Diversity

A significant increase in the taxon richness and diversity of radiolarian assemblages can be seen from Termination I to the present. Whether this is due to climate-related changes in living radiolarian assemblages over time, or due to preservation bias, is unclear. It is possible that during climatically unstable transition periods, radiolarian assemblages tend to be more specialised and, therefore, less diverse. During periods of high radiolarian abundance, the ratio of nassellarian to spumellarian species is high, and the ratio of *C. davisiana* to *S. arachnea* is low. Specifically, *C. davisiana* RA values are strongly negatively correlated with radiolarian TA, a result consistent with observations by Matsuzaki et al. (2014). The generally high RNS values in both cores are atypical with core-tops in this region generally having a more spumellarian rich, pelagic assemblage rather than a nassellarian rich coastal assemblage (Nishimura and Nakaseko, 2011). Collection of samples closer to the Antarctic continent to compare RNS would allow for establishing typical coastal/pelagic RNS values for this region. Investigating the diversity of radiolarian assemblages through multiple glacial cycles will be necessary to provide evidence of whether trends observed during Termination I and the Holocene are similar across multiple glacial/interglacial cycles.

3.4.4 Timing of observed events

Foraminifera-based ^{14}C dating of KC05 samples placed the 220 cm layer at ~33.8 ka (+/- 0.35). No ^{14}C dates are available for core KC11. Assuming a constant rate of sedimentation from 0 – 220 cm, the sedimentation rate for KC05 is 6.5 cm/ ka. The constant sedimentation rate (CSR) model places peak TA and RNS at ~4 ka, peak *C. davisiana* abundance and RCS at ~8.6 ka, and the near disappearance of radiolarians at this site at ~10.2 ka. The small peak in radiolarian abundance at 209 cm would have occurred at ~32.2 ka (Table 4). By using the peaks in *C. davisiana* RA, a more accurate age model may be obtained. Matsuzaki et al. (2014) identified 20 *Davisiana* stratigraphic events (DAE's) based on peaks in *C. davisiana* RA in a core taken from a location East of the Shimokita Peninsula, Japan. DAE 2 occurred at 12 ka, while DAE 3 occurred at 17 ka. DAE 3 matches best with the Antarctic 'b' event identified by Hays et al. (1976) in Southern Ocean sediments which was

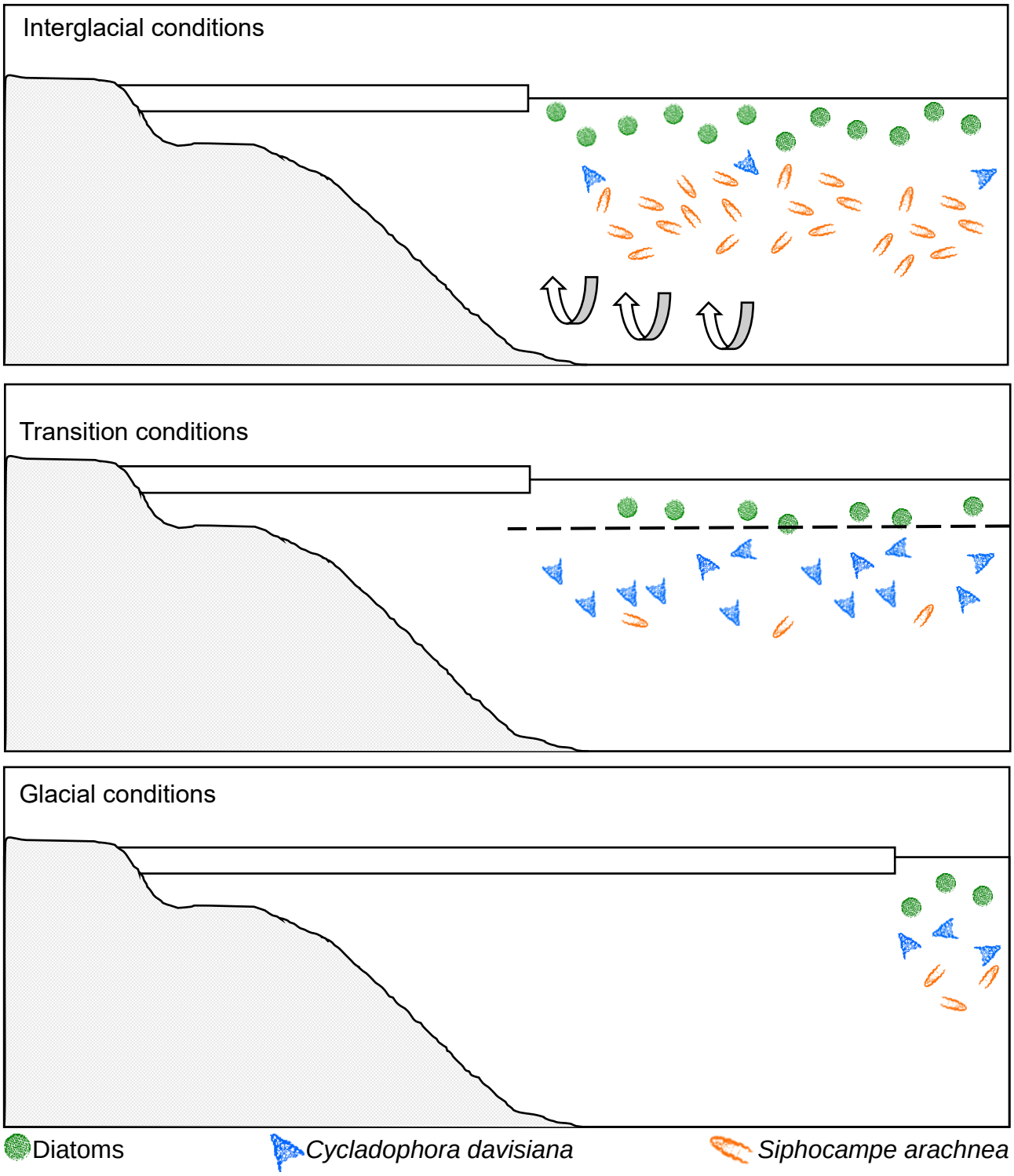

Figure 11: Conditions during the three main stages identified using radiolarian assemblages: interglacial, transition and glacial. Year-round sea ice coverage was present at the survey site during the last glacial period, with virtually no biosiliceous sediment obtained. During the transition period, Termination I, sea ice retreated, the water column became highly stratified and *Cycladophora davisiana* relative abundance peaked. During the current interglacial, the Holocene, the ratio of *C. davisiana* to *Siphocampe arachnea* was lower and the water column became mixed due to upwelling.

dated at between 14-24 ka. If we assume that DAE 3 matches up with peak *C. davisiana* RA in KC05 the sedimentation rate between 0 – 51 cm (i.e. between 17 ka and the present) is ~3 cm/ ka, while from 51-220 cm (the 17-33.8 ka time interval) the sedimentation rate is ~10.1 cm/ ka. This places peak TA and RNS at ~8.7 ka, peak *C. davisiana* abundance and RCS at ~17.5 ka and the near disappearance of radiolarians at this site at ~18.5 ka. The small peak in radiolarian abundance at 209 cm would have occurred at ~32.6 ka.

It is, however, worth noting that the Hays et al. (1976) cores were significantly further north (~45ºS) than KC05 (~65°S) and that at 17 ka the KC05 site was likely to have been permanently sea-ice covered (Gersonde et al., 2005). In this case, peak *C. davisiana* RA seen in KC05 may have coincided with DAE 2 at 12 ka. If so, the sedimentation rate between 0 – 51 cm (i.e. between 12 ka and the present) is ~4.3 cm/ ka, while from 51-220 cm (12-33.8 ka) the sedimentation rate is ~7.8 cm/ ka. This places peak TA and RNS at ~6.1 ka, peak *C. davisiana* abundance and RCS at ~12.6 ka and the near disappearance of radiolarians at this site at ~13.9 ka. The small peak in radiolarian abundance at 209 cm would have occurred at ~32.4 ka.

Table 4: The estimated timing of notable assemblage events in KC05 based on three age models: one based on a constant sedimentation rate (CSR) from 0-220 cm, and two incorporating the alignment of peak KC05 C. davisiana with Davisiana Events (DAE) 3 and 2 respectively.

Event	Estimated timing per model (Ka)		
	CSR	DAE 3	DAE 2
Peak TA/RNS	4	8.7	6.1
Peak *C. davisiana* RA/ RCS	8.6	17.5	12.6
TA drop off	10.2	18.5	13.9
209 cm peak	32.2	32.6	32.4

The depth at which the boundaries between MIS 3/2 and MIS 2/1 (29 ka and 14 ka respectively) (Lisiecki and Raymo, 2005) occurred have been estimated according to the three age model scenarios (Fig. 12). The most plausible age model is that which is based on the timing of DAE 2. In this scenario, peak *C. davisiana* RA occurred shortly after the MIS 2/1 boundary, as would be expected given the knowledge regarding *C. davisiana* peak abundance patterns. Evidence provided by Gersonde et al. (2005), which suggests the study region was covered by year-round sea ice during the last glacial maximum (19.5 – 16 ka), invalidates the DAE 3 model which has *C. davisiana* peaking at 17.5 ka, while the CSR model has *C. davisiana* peaking well into the Holocene.

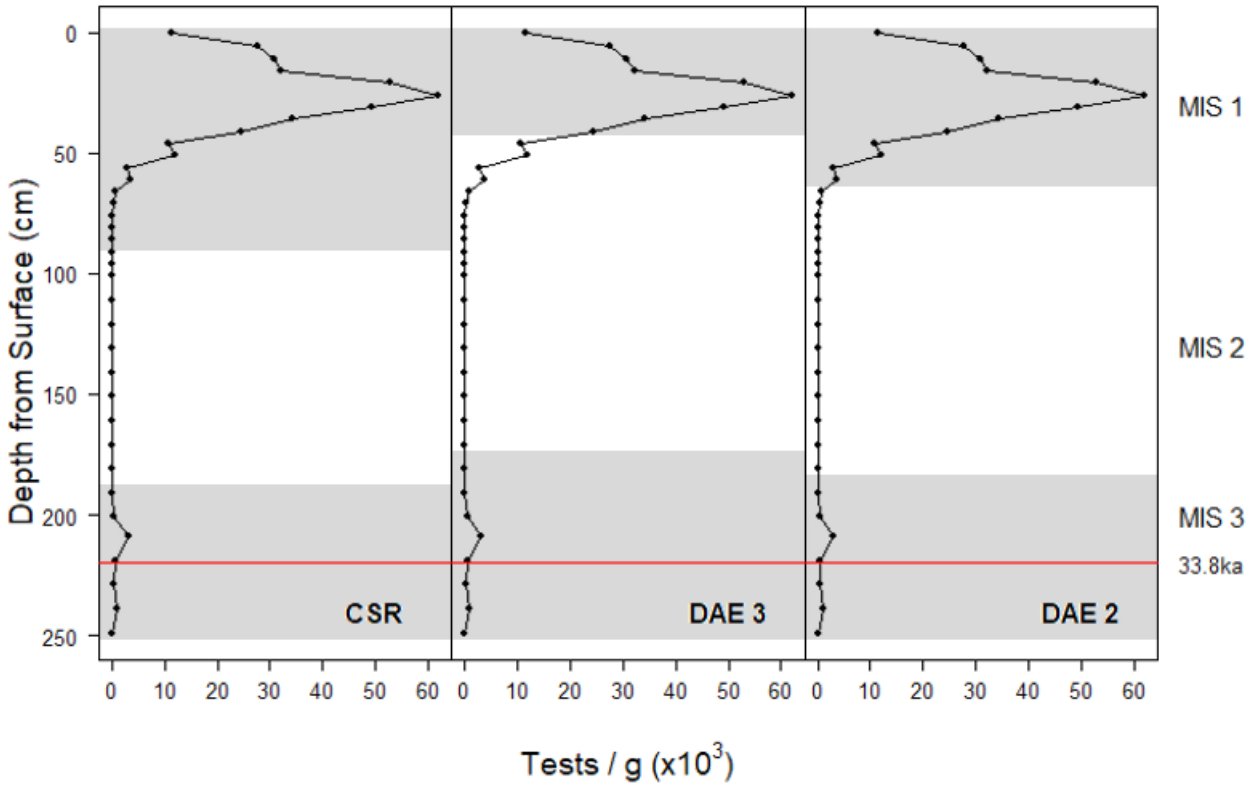

Figure 12: Radiolarian total abundance and marine isotope stages (shaded) for KC05 according to three different age models. L-R: The constant sedimentation rate (CSR), Davisiana Event (DAE) 3 and DAE 2 models. The DAE 2 model may fit best with the peak in *C. davisiana* abundance (51 cm) occurring at 12.6 ka, shortly after Termination I (67 cm, 14 ka).

3.4.5 KC05-209

The lone sample in the lower part of KC05 that had a high enough TA to obtain assemblage data was classified into its own cluster. The radiolarian assemblage observed in this sample had an unusually high percentage of *C. davisiana* (~30%) and was dated at ~32-33 ka by all three age models. The lack of radiolarians in the samples 10 cm either side of KC05-209 make it impossible to determine oceanic conditions during these intervals of deposition. More information may be obtained through higher resolution sampling, or by sampling longer cores from the region. A ~16 m piston core retrieved from the same ridge as KC05 (Armand et al., 2018) is likely to contain sediment from several more glacial/interglacial cycles. If a similar peak is seen at a similar time interval, then an opportunity exists for higher resolution sampling and the potential to determine earlier changes to the oceanic conditions across the slope environment.

4. Radiolarian-based palaeotemperature estimates for the current interglacial

4.1 Introduction

In the previous section, it was shown that KC05 and KC11, the two cores on which this study focusses, contain sediment from marine isotope stages 1 - 3. Only the upper parts of each core, which are interpreted as being representative of the Holocene and of glacial Termination I, are abundant in radiolarians and, therefore, are suitable for assemblage-based palaeotemperature reconstruction. The lower sections of the two cores lack radiolarians and thus it is not possible to reconstruct palaeo-SST based on radiolarians in those earlier intervals.

4.1.1 Palaeotemperature reconstruction

Reconstructing ocean palaeotemperature based on microfossil assemblage data uses what is known about the biology and ecology of extant radiolarian species to infer what conditions were like when, and where, they lived in the past. The abundance and composition of marine microfossils such as foraminifera (Labracherie et al., 1989; Niebler and Gersonde, 1998; Pichon et al., 1987), diatoms (Benz et al., 2016; Crosta et al., 2004; Gersonde et al., 2005) and radiolarians (Cortese and Abelmann, 2002; Cortese and Prebble, 2015; Rogers and De Deckker, 2011) have been used to reconstruct palaeoclimate parameters such as SST and sea ice extent in the Southern Ocean.

Several biological assumptions are made when reconstructing palaeotemperature based on radiolarian assemblages. Similar assumptions apply when attempting palaeotemperature reconstructions using any microfossil group.

1. Knowledge of extant radiolarian ecology and geographic distribution are sufficient to interpret the fossil data (Guiot and de Vernal, 2007) i.e. the knowledge of the biology and environmental affinity of the radiolarian species found in sediment samples are both extensive and accurate.
2. The climatic/environmental affinity of the species has not changed over time (Guiot and de Vernal, 2007) i.e. extant radiolarian species currently live in water masses which have the same characteristics as those water masses that they have always lived in.
3. Climate is the primary cause of changes in the radiolarian assemblage over time (Guiot and de Vernal, 2007), specifically, in this case, that changes in sea temperature are the main cause of changes to the radiolarian assemblage.

4. The radiolarian assemblage found in seafloor sediment is an accurate representation of the assemblage which once lived in the overlying water column (Abelmann and Gowing, 1997). i.e. there has been no significant horizontal transport or selective dissolution of radiolarian tests as they have settled through the water column and no significant reworking of sediments once they have settled.

When extinct radiolarian species appear in sediment samples, the biology and ecology of the assemblage becomes uncertain and the first biological assumption is violated (Kucera, 2015).

4.2 Methods

4.2.1 Imbrie-Kipp Transfer Function

Transfer functions use palaeontological data to produce reliable, quantitative estimates of environmental parameters. First published in 1971 by Imbrie and Kipp, and originally developed using planktonic foraminifera data, the Imbrie-Kipp transfer function method (IKM) has since been used with proxies such as fossilised pollen, benthic foraminifera, diatoms, nannofossils and radiolarians (Guiot and de Vernal, 2007). The IKM consists of three steps. The first involves performing principal components analysis (PCA) on a core top assemblage dataset which represents the modern assemblage likely to be preserved in the fossil record. PCA reduces a large number of observed variables (in this case, species abundance data at multiple “modern” sites) to a few linearly uncorrelated factors (Tabachnick and Fidell, 2013). The second step uses the core-top derived factors in a multiple regression to establish a relationship between modern assemblages and modern observations of an environmental variable, such as SST. The result is a calibration equation/transfer function relating ecological assemblages to the environmental variable. Palaeotemperatures are estimated in the third step when past assemblage data from a core is projected on the principal components from the modern assemblage dataset and the resulting factor scores are entered into the calibration equation (Guiot and de Vernal, 2007; Imbrie and Kipp, 1971).

As well as the IKM, other methods for deriving palaeotemperature estimates have been used in conjunction with fossil radiolarians, e.g. the modern analogue technique and artificial neural networks. IKM was chosen for this study after a review of radiolarian-based palaeotemperature estimates published in the last ten years found IKM is still the most utilised technique, despite its age (Supplement D). The widespread use of this technique

was seen to be a positive, and it may be that other techniques will be employed using this dataset in the future.

Palaeotemperature estimates for KC05 and KC11 were calculated using the PaleoToolbox application (Sieger et al., 1999). To perform IKM using PaleoToolbox, three input files were generated: a reference file containing core top assemblage data, an environment file containing modern SST measurements and a core file containing the box core palaeo assemblages. The reference file consisted of radiolarian RA from 55 core tops - 8 core tops collected during IN2017-V01 (KC07 was excluded due to the very low radiolarian TA at this site) and 47 core tops from the modern analogue dataset published by Cortese and Prebble (2015) (Fig. 13; Table 5). Of the 88 core tops included in that study, only the 47 core tops from south of 40°S were included in the reference file.

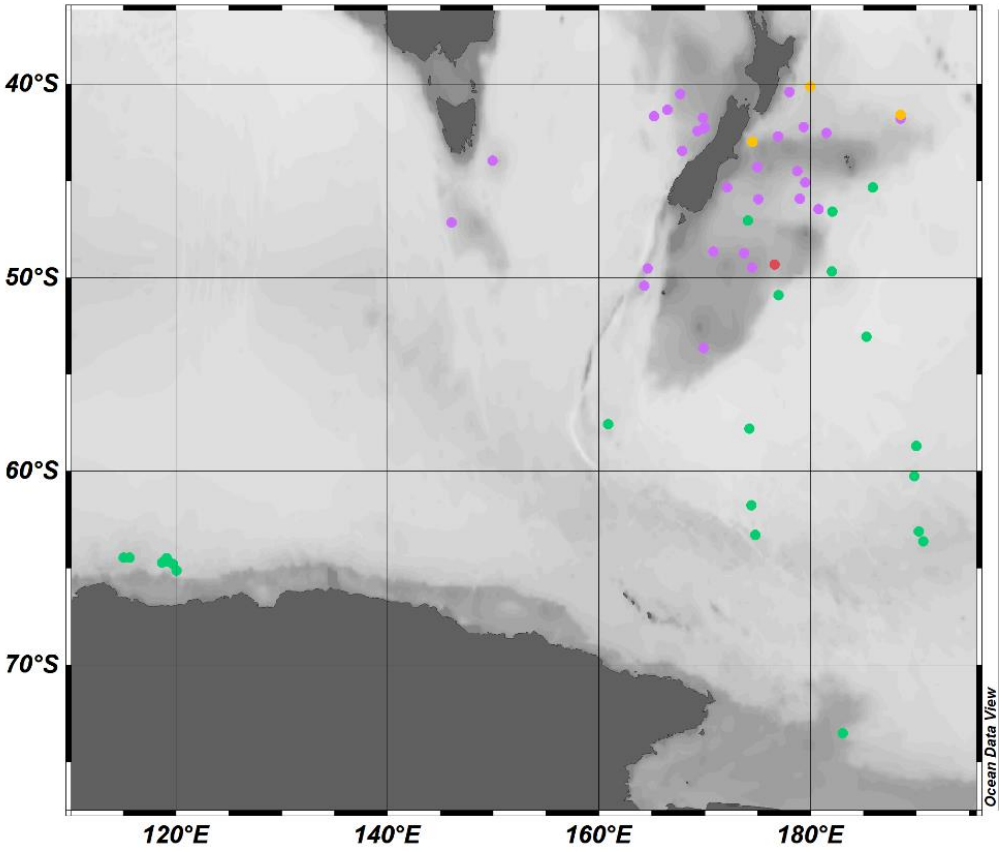

Figure 13: Core tops contained in the IKM reference file coloured according to which factor has the highest score at each core top location. Core tops from this study are influenced by Factor 2 (green). Factor 2 includes all samples south of -55°S, and several samples further north, covering an area with a very broad SST range.

The environment file contained the average summer SST (SSST) for each core top site. Average SSST, rather than average annual SST, was used as ~90% of radiolarian production occurs during the summer months (Abelmann and Gersonde, 1991), therefore

temperature estimates should not be extrapolated beyond this. The 1955 – 2012 average monthly SST data for December - March were retrieved from the World Ocean Atlas 2013 dataset (Locarnini et al., 2013) at a resolution of 0.25° and were accessed using Ocean Data View (Schlitzer, 2002) software. The daily weighted average SST from December - March was used to calculate the average SSST for the environment file.

The core file contained RA data from the KC05 (n=14) and KC11 (n=24) C-slide counts (excluding core tops as these were already included in the reference dataset). Taxa with <1% RA in the analysis dataset were excluded from both the reference and core files. Of the remaining taxa, five (*Acanthodesmia micropora*, *Actinomma kerguelensis*, *Cladoscenium tricolpium*, *Euphysetta staurocodon* and *Rhizoplegma boreale*) were not found at any sites in the Cortese and Prebble (2015) dataset so could not be included in the IKM calculations. Three taxa recorded in IN2017-V01 samples, *Larcopyle pylomaticus*, *Larcopyle weddellium* and *Phormospyris stabilis antarctica*, were found under synonyms, *Spongurus pylomaticus*, *Spongurus* spp. and *Triceraspyris antarctica* respectively, in the Cortese and Prebble (2015) dataset. Thirty-five taxa were included in the final core and reference files (Supplement B). Using PaleoToolbox (Sieger et al., 1999), IKM was run with 5-factors to produce a quadratic regression equation, palaeo-SSST estimates and their residuals for the core tops in the reference dataset, and palaeo-SSST estimates for each box core sample.

4.3 Results

4.3.1 Factor analysis

Factor analysis of the reference dataset shows that the first five factors account for 92% of the variance found in the core top assemblages with 78% of the variance accounted for by the first two factors (Table 6).

Factor 1 (F1) accounts for 40% of core top assemblage variance and is heavily influenced by *Stylodictya aculeata/validispina* (scaled varimax factor score (SVFS) 5.623), a taxon having an average RA of 1.29% in KC05 and 0.96% in KC11.

Factor 2 (F2) accounts for 38% of the variance and is heavily influenced by *Antarctissa* spp. (SVFS 5.479) which has an average RA of 24.76% in KC05 and 24.45% in KC11 and is the dominant species in all IN2017-V01 core top and box core samples excluding KC05-209.

Factor 3 (F3) accounts for 7% of the variance and is influenced by *Botryostrobus auritus-australis* and *Larcopyle weddellium* (SVFS 3.734 and 2.347 respectively). *B. auritus-*

Table 5: Reference dataset used in summer SST estimates. Basic core top station information is given, along with communality (Comm.) and factor scores for each station in the reference dataset. The variance explained by each of the factors (F1-5), as well as the cumulative variance, is also shown. Factor values in bold are the highest for that core top

** indicates that core top was collected during IN2017-V01. All other core tops are from the Cortese and Prebble dataset (2015).*

Station	Longitude	Latitude	Depth (m)	SST (°C)	Comm.	F1	F2	F3	F4	F5
B32	169.87	-53.63	799	8.84	0.91	**0.809**	0.05	0.164	0.471	-0.069
DSDP593A	167.68	-40.51	376	17.54	0.95	**0.945**	0.026	0.205	-0.113	-0.036
F104	170.81	-48.67	801	11.09	0.813	**0.686**	0.044	0.151	0.562	-0.041
F150	174.47	-49.47	501	9.94	0.883	**0.65**	0.237	0.112	0.573	0.252
F755	174.50	-43.00	854	15.53	0.762	0.407	0.08	**0.729**	0.243	-0.011
G944	179.99	-40.12	2890	18.48	0.866	0.545	0.135	**0.737**	-0.053	0.068
H550	180.76	-46.45	3528	13.27	0.909	0.57	**0.569**	0.131	0.248	-0.427
H555	178.98	-45.92	2738	13.60	0.936	**0.822**	0.117	0.188	0.455	0.06
H564	174.08	-47.04	1429	12.38	0.941	0.275	**0.87**	0.053	0.199	-0.258
J1049	178.73	-44.50	1339	14.33	0.976	**0.908**	0.357	0.024	0.127	0.078
KC03 *	115.04	-64.46	1862	-0.36	0.963	0.045	**0.974**	-0.05	0.017	-0.097
KC04 *	119.30	-64.68	3103	0.08	0.958	0.047	**0.961**	0.108	0.022	-0.139
KC05 *	119.02	-64.65	3198	0.07	0.944	0.075	**0.945**	0.182	0.041	-0.098
KC06 *	118.70	-64.73	3320	-0.02	0.952	0.047	**0.971**	0.072	0.005	-0.04
KC08 *	119.74	-64.79	3282	0.03	0.957	0.017	**0.973**	-0.035	-0.024	-0.091
KC11 *	120.05	-65.13	3354	-0.22	0.894	0.104	**0.926**	0.122	-0.029	0.099
KC13 *	119.10	-64.48	2612	0.20	0.947	0.082	**0.967**	0.044	0.027	-0.047
KN01BC	173.73	-48.73	3321	10.58	0.844	**0.759**	0.174	0.192	0.393	0.215
KN02BC	174.23	-57.81	5344	6.68	0.926	0.146	**0.946**	0.02	0.044	0.082
KN04BC	174.42	-61.77	4240	3.94	0.973	0.072	**0.974**	0.003	0.002	0.139
KN06BC	174.78	-63.29	2429	2.15	0.971	0.02	**0.981**	-0.048	0.058	0.054
KN11BC	-169.32	-63.63	2738	0.86	0.944	0.033	**0.952**	0.037	-0.009	0.186
MC01 *	115.62	-64.47	2161	-0.31	0.955	0.047	**0.975**	0.013	-0.027	-0.022
NBPMC1	-176.96	-73.54	561	-1.12	0.896	0.04	**0.844**	0.031	0.104	0.412
NBPMC10	-174.69	-53.04	5470	9.66	0.894	0.229	**0.84**	0.259	0.258	-0.051
NBP05MC1	-169.74	-63.11	2927	1.19	0.976	0.039	**0.986**	-0.027	0.002	0.051
NBP07MC1	-170.19	-60.24	3860	3.53	0.965	0.033	**0.932**	-0.003	0.056	0.303

Station	Longitude	Latitude	Depth (m)	SST (°C)	Comm.	F1	F2	F3	F4	F5
NBP08MC1	-169.98	-58.69	4324	4.52	0.979	0.041	**0.988**	-0.028	0.013	0.012
ODP1121A	177.00	-50.90	4492	8.92	0.925	0.125	**0.952**	0.019	0.036	0.044
ODP1123B	-171.50	-41.79	3290	16.77	0.928	**0.896**	0.117	0.322	-0.018	-0.083
ODP1170C	146.05	-47.15	2703	11.50	0.981	**0.978**	0.101	0.062	0.01	-0.097
ODP1172C	149.93	-43.96	2611	15.07	0.889	**0.934**	0.078	0.105	-0.01	-0.011
P69	177.99	-40.40	2195	18.49	0.8	**0.808**	0.048	0.348	-0.102	-0.115
P933	165.22	-41.66	4421	17.21	0.768	**0.615**	0.1	0.611	0.081	0.026
P937	166.46	-41.32	3253	17.40	0.892	**0.762**	0.052	0.548	0.032	-0.085
Q203	175.06	-45.96	1668	13.32	0.856	**0.671**	0.237	0.308	0.336	-0.377
Q220	174.98	-44.29	580	14.27	0.958	**0.964**	0.059	0.006	0.121	-0.102
Q575	185.92	-45.33	4680	14.45	0.952	0.318	**0.845**	0.242	0.16	-0.23
Q582	182.08	-46.60	4440	13.55	0.931	0.306	**0.847**	0.077	0.057	-0.332
Q585	182.01	-49.67	4500	10.55	0.966	0.316	**0.814**	0.157	0.368	-0.211
Q689	170.01	-42.25	948	18.02	0.885	**0.926**	0.021	0.147	0.07	0.039
Q699	169.30	-42.42	698	17.84	0.89	**0.931**	0.024	-0.11	-0.047	0.091
Q720	169.84	-41.73	960	17.92	0.943	**0.957**	0.005	0.044	0.152	-0.039
R657	181.51	-42.53	1408	16.92	0.943	**0.943**	0.025	0.216	0.025	-0.073
S631	172.11	-45.33	1329	12.87	0.954	**0.876**	0.263	-0.027	0.334	0.073
S924	188.50	-41.58	3550	16.88	0.947	0.669	0.104	**0.683**	0.001	-0.147
SO136-005	169.87	-42.31	958	17.99	0.937	**0.963**	0.041	-0.076	0.011	0.043
SO136-011	167.85	-43.44	1556	16.89	0.967	**0.966**	0.049	0.167	0.009	0.053
Tan0333	176.61	-49.32	1433	9.64	0.807	0.492	0.246	-0.007	**0.701**	-0.116
Tan08127	160.87	-57.56	3830	4.36	0.919	0.034	**0.953**	-0.05	0.006	-0.085
Tan0827	164.61	-49.52	3250	10.69	0.871	**0.838**	0.06	0.153	0.364	-0.093
Tan0840	164.29	-50.43	3524	10.17	0.96	**0.883**	0.092	0.204	0.341	-0.12
U938	179.51	-45.08	2700	14.18	0.932	**0.916**	0.229	0.088	0.097	-0.153
U951	176.91	-42.72	850	16.24	0.853	**0.787**	0.05	0.479	0.045	-0.014
W266	179.36	-42.22	2540	17.16	0.873	**0.835**	0.027	0.417	-0.013	-0.028
					VARIANCE (%)	39.85	38.03	6.5	4.94	2.34
					CUM. VAR (%)	39.85	77.88	84.38	89.32	91.66

australis has an average RA of 1.91% in KC05 and 2.17% in KC11, while *L. weddellium* has an average RA of 2.69% in KC05 and 1.46% in KC11.

Factor 4 (F4) accounts for 5% of the variance and is influenced by *Spongopyle osculosa/resurgens, Lithomelissa boreale* gr*.* and *Phorticium clevei* (SVFS 3.907, 2.426 and 2.137 respectively). *S. osculosa/resurgens* has an average RA of 1.05% in KC05 and 0.73% in KC11, *L. boreale* gr*.* has an average RA of 0.12% in KC05 and 0.24% in KC11 and *P. clevei* has an average RA of 0.40% in KC05 and 0.45% in KC11.

Factor 5 (F5) accounts for 2% of the variance and is influenced by the differences in the abundance of *L. boreale* gr. and *S. arachnea*, and *C. davisiana* (SVFS 2.859, 2.726 and -2.612). *Siphocampe arachnea* has an average RA of 4.84% in KC05 and 6.13% in KC11, while *C. davisiana* has an average RA of 6.21% in KC05 and 5.55% in KC11. Since *L. boreale* gr. accounts for a fraction of a percentage of RA in the box core samples (see F4, above), F5 shall be simply considered as the contrast between *C. davisiana* and *S. arachnea* – two species which had a strong influence on the cluster analysis results in the previous section*.*

Table 6: Scaled varimax factor scores (SVFS) for taxa which had at least one factor loading >|2|. Large SVFS are in bold indicating the corresponding taxa are an important species to that factor. Full IKM species list, including factor loadings, can be found in Supplement E.

Taxa	**F1**	**F2**	**F3**	**F4**	**F5**
Antarctissa spp*.*	-0.07	**5.479**	-0.777	-0.227	-0.514
Botryostrobus auritus-australis	0.267	0.081	**3.734**	-0.268	0.354
Cycladophora davisiana davisiana	-0.095	1.078	0.499	0.228	**-2.612**
Larcopyle weddellium	0.188	0.36	**2.347**	-0.679	-0.93
Lithomelissa boreale gr*.*	0.039	0.437	0.338	**2.426**	**2.859**
Phorticium clevei	0.186	0.157	-0.479	**2.137**	-1.936
Siphocampe arachnea	0.099	1.258	0.455	-0.583	**2.726**
Spongopyle osculosa/resurgens	1.23	0.042	-0.026	**3.907**	0.042
Stylodictya aculeata/validispina	**5.623**	0.026	-0.217	-1.055	-0.213

4.3.2 Palaeotemperature estimates

Reference dataset

Using the calibration equation (Table 7) provided by the IKM, core top SSST estimates (standard error ±1.97 °C) were generated for the core top reference dataset, as well as the residuals for observed vs estimated SSST calculated (Table 8). Comparing the estimated and observed core top SSST measurements for corresponding sites allows the performance of the transfer function to be validated. The observed SSST vs estimated SSST plot shows no obvious bias in over/underestimating core top SSST, and the observed SSST vs residuals plot shows most of the residuals fall within ±2 °C (Fig. 14).

Table 7: Regression terms and coefficients for the palaeotemperature calibration equation generated using IKM.

Regression Term	Regression Coefficient
$F1^2$	4.415
$F2^2$	82.733
$F3^2$	27.691
$F4^2$	-15.647
$F5^2$	17.660
F1*F2	99.726
F1*F3	49.173
F1*F4	-9.227
F1*F5	26.360
F2*F3	40.528
F2*F4	22.004
F2*F5	25.761
F3*F4	1.196
F3*F5	18.874
F4*F5	6.172
F1	-34.775
F2	-130.457
F3	-57.889
F4	-0.890
F5	-26.623
Intercept	47.101

*Table 8: Observed and estimated summer SST, and residuals, for each core top in the reference dataset. * indicates that core top was collected during IN2017-V01.*

Station	Observed SST (°C)	Estimated SST (°C)	Residual
B32	8.84	10.83	-1.99
DSDP593A	17.54	17.07	0.47
F104	11.09	11.73	-0.64
F150	9.94	9.65	0.29
F755	15.53	15.06	0.47
G944	18.48	17.33	1.15
H550	13.27	14.06	-0.79
H555	13.60	10.05	3.55
H564	12.38	12.79	-0.41
J1049	14.33	15.79	-1.46
KC03*	-0.36	2.83	-3.19
KC04*	0.08	0.10	-0.02
KC05*	0.07	0.82	-0.75
KC06*	-0.02	0.42	-0.44
KC08*	0.03	0.03	0.00
KC11*	-0.22	1.65	-1.87
KC13*	0.20	3.30	-3.10
KN7812 01BC	10.58	12.39	-1.81
KN7812 02BC	6.68	7.37	-0.69
KN7812 04BC	3.94	3.43	0.51
KN7812 06BC	2.15	2.00	0.15
KN7812 11BC	0.86	-0.42	1.28
MC01*	-0.31	0.75	-1.06
NBP MC1	-1.12	0.83	-1.95
NBP MC10	9.66	8.64	1.02
NBP9802 05MC	1.19	1.89	-0.70
NBP9802 07MC	3.53	1.57	1.96
NBP9802 08MC	4.52	2.31	2.21
ODP1121A	8.92	6.01	2.91
ODP1123B	16.77	15.49	1.28
ODP1170C	11.50	14.38	-2.88
ODP1172C	15.07	15.50	-0.43
P69	18.49	17.95	0.54
P933	17.21	16.94	0.27
P937	17.40	18.30	-0.90
Q203	13.32	11.59	1.73
Q220	14.27	14.71	-0.44
Q575	14.45	12.66	1.79
Q582	13.55	12.15	1.40
Q585	10.55	12.30	-1.75
Q689	18.02	16.22	1.80
Q699	17.84	19.45	-1.61
Q720	17.92	15.47	2.45
R657	16.92	16.04	0.88

Station	Observed SST (°C)	Estimated SST (°C)	Residual
S631	12.87	12.17	0.70
S924	16.88	18.21	-1.33
SO136-005	17.99	17.13	0.86
SO136-011	16.89	15.67	1.22
Tan0307-33	9.64	9.10	0.54
Tan0803-127	4.36	1.34	3.02
Tan0803-27	10.69	12.30	-1.61
Tan0803-40	10.17	11.13	-0.96
U938	14.18	13.22	0.96
U951	16.24	17.82	-1.58
W266	17.16	18.18	-1.02

KC05

KC05 downcore SSSTs estimated using the IKM ranged between -2.2 °C (26 cm) and 3.3 °C (11 cm) (Table 9). The palaeotemperature signal is dominated by *Antarctissa* spp. with the F2 value for all sample depths (excluding KC05-209) being greater than 0.9. Secondary influences were identified by looking for factor loadings with an absolute value greater than 0.1. The 6 cm sample showed a contribution from F3 (indicative of *B. auritus-australis* and *L. weddellium* influencing estimated SSST) and several depths showing some contribution from F5 (indicative that the contrast in abundance between *S. arachnea*, and *C. davisiana* impact the estimated temperatures). KC05-209 is the sample most different from the rest with an unusually low F2 value and an unusually high F5 value – explained by the relatively low *Antarctissa* spp. RA and relatively high *C. davisiana* RA in this sample.

No correlations between palaeo-SSST estimates and diversity indices were statistically significant for KC05, however RNS had a relatively strong negative correlation with palaeo-SSST (r = -0.51, p = 0.062) (Fig. 15). The correlation between palaeo-SSST and TA was also not statistically significant (r = -0.329, p = 0.251).

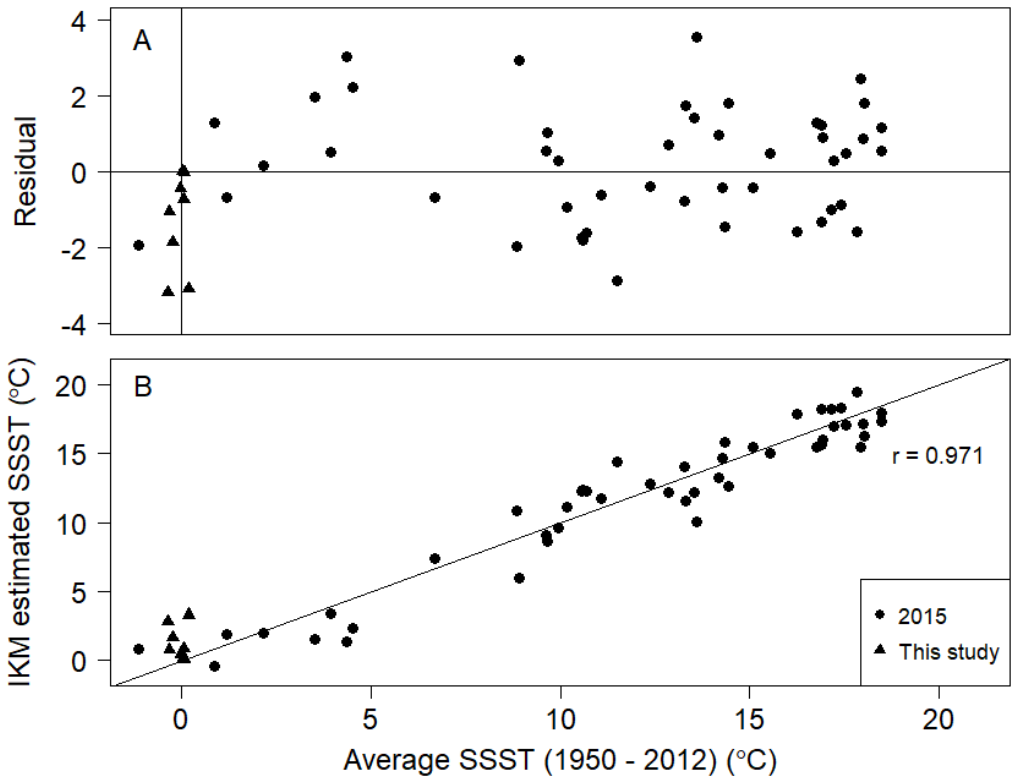

Figure 14: *A.* Residuals of core top SSST vs observed SSST and *B.* observed SSST vs estimated palaeo-SSST (Pearson's r = 0.971, p < 0.001).

Table 9: Estimated palaeo-SSST for KC05. NA communality values indicate No Analog conditions. Factor loadings and cluster membership are also reported.

Depth (cm)	Comm.	Est. SST (°C)	F1	F2	F3	F4	F5	Cluster
0	0.944	0.82	0.075	**0.945**	**0.182**	0.041	-0.098	1
6	NA	-1.09	0.0503	**0.9613**	**0.1121**	-0.0436	0.0382	1
11	0.9729	3.26	0.096	**0.9709**	0.0942	-0.0017	**-0.1105**	1
16	0.9484	1.93	0.0853	**0.9669**	0.0672	-0.0395	-0.012	1
21	0.9483	-0.16	0.0513	**0.9641**	0.0982	-0.0209	0.0775	1
26	0.9327	-2.24	0.0276	**0.9485**	0.0894	-0.0344	**0.1519**	1
31	NA	1.11	0.0487	**0.9689**	0.0384	0.0081	0.0799	2
36	0.9729	0.89	0.0395	**0.9839**	0.0347	0.0029	-0.0469	1
41	NA	1.91	0.0459	**0.9766**	0.0159	0.0306	-0.0686	3
46	NA	-1.63	0.0019	**0.9437**	0.0578	0.0238	**-0.2289**	3
51	NA	-0.86	0.0355	**0.9306**	0.0785	0.0137	**-0.2006**	3
56	NA	1.83	0.0804	**0.9271**	0.0864	0.0247	**-0.2285**	3
61	NA	1.06	0.0486	**0.9298**	0.0565	0.0559	**-0.2138**	3
66	NA	3.17	0.0719	**0.962**	0.015	0.0182	**-0.1743**	3
209	NA	2.90	0.0136	**0.6294**	0.094	0.0447	**-0.44**	4

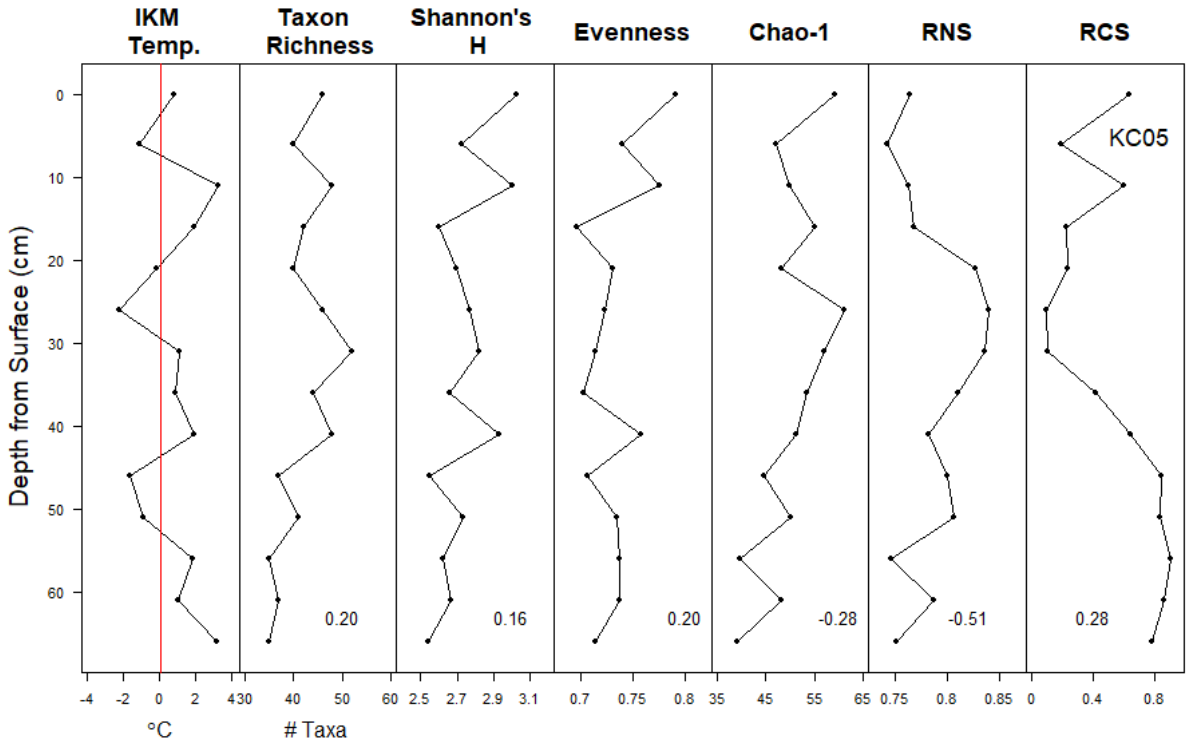

Figure 15: Palaeo-SSST estimates for KC05. Vertical red line indicates the average modern SSST for the site. Diversity indices are plotted with Pearson's r values showing the correlation between the index and palaeo-SSST, none of which were statistically significant.

KC11

Estimates of palaeo-SSST for KC11 using the IKM ranged between -3.3 °C (53 cm) and 2.7 °C (138 cm) (Table 10). Like KC05, the palaeotemperature signal is dominated by *Antarctissa* spp. with the F2 value for all sample depths being greater than 0.9. Several samples have some contribution from F3 (indicative of a contribution by *B. auritus-australis* and *L. weddellium*) and several depths show a contribution by F5 (indicative that the contrast in abundance between *S. arachnea*, and *C. davisiana* has some influence). The 13 cm depth is influenced by both F3 and F5, however due to the factor being positive (0.1354) it indicates a higher *S. arachnea*, rather than *C. davisiana*, abundance.

Palaeo-SSST and RNS are significantly negatively correlated in KC11 (r = -0.50, p = 0.01) (Fig. 16). Correlations between palaeo-SSST estimates and the remaining diversity indices, including TA (r = -0.134, p = 0.523), are not statistically significant.

Table 10: Estimated palaeo-SSST for KC11. NA communality values (Comm.) indicate No Analog conditions. Varimax Factor Loadings and cluster membership are also reported.

Depth (cm)	Comm.	Est. SST (°C)	F1	F2	F3	F4	F5	Cluster
0	0.894	1.65	0.104	**0.926**	**0.122**	-0.029	0.099	1
3	NA	-0.02	0.0548	**0.9524**	**0.1046**	0.0068	0.0341	1
8	NA	0.14	0.0886	**0.9172**	**0.1461**	-0.0223	0.0778	1
13	NA	-1.06	0.0578	**0.9134**	**0.1229**	0.0044	**0.1354**	1
18	0.9565	0.88	0.0745	**0.967**	**0.1134**	-0.0394	0.0365	1
23	NA	0.19	0.0589	**0.9586**	0.063	-0.0348	0.0736	1
28	NA	-1.16	0.0335	**0.9721**	0.0657	-0.0355	0.0239	1
33	NA	2.44	0.0585	**0.9796**	-0.0051	-0.0018	0.0071	1
38	NA	-2.13	0.0466	**0.9416**	**0.1324**	-0.0445	0.0836	1
43	NA	0.40	0.0278	**0.9695**	-0.0515	-0.0306	0.091	2
48	NA	-1.21	0.0296	**0.9635**	0.0834	-0.0068	0.0812	2
53	NA	-3.26	0.0135	**0.9521**	**0.1008**	-0.0244	0.0843	2
58	NA	-2.07	0.0068	**0.966**	0.0365	-0.0066	0.0027	2
63	NA	-0.84	0.0294	**0.968**	0.0339	-0.0235	0.0584	2
68	NA	-1.57	0.0176	**0.9697**	0.069	0.0013	0.0209	2
73	NA	0.25	0.0474	**0.976**	0.077	-0.0133	-0.0842	2
78	NA	-3.14	0.0142	**0.9422**	0.0831	-0.0297	**-0.1311**	3
83	NA	-0.24	0.0315	**0.9678**	0.0347	-0.011	**-0.1153**	3
88	NA	-0.61	0.0312	**0.9605**	0.0375	-0.0135	**-0.1059**	3
93	NA	-1.29	0.0294	**0.9373**	0.0574	-0.012	**-0.1779**	3
98	NA	-0.98	0.0141	**0.9494**	0.0395	0.008	**-0.1985**	3
108	NA	0.09	0.0314	**0.9485**	0.0455	0.0141	**-0.214**	3
118	NA	-1.00	0.0229	**0.9807**	0.0454	-0.022	-0.0068	1
128	NA	-0.38	0.049	**0.961**	**0.1233**	0.0058	-0.095	1
138	NA	2.69	0.0784	**0.937**	0.0489	0.0372	**-0.2063**	3

Five KC05 samples (36% of the total number of samples analysed at this site) and 15 KC11 samples (60% of the total) have palaeo-SSSTs which are cooler than the modern mean SSST calculated for each of the two sites. The mean palaeo-SSST for Cluster 1 samples was 0.17 °C, for Cluster 2 samples was -0.90 °C and for Cluster 3, 0.15 °C. Mean palaeo-SSST does not differ significantly between clusters (ANOVA, $F = 1.35$, $p = 0.272$).

In both cores, large negative F5 values coincide with the sorting of these samples into Cluster 3 and further illustrate that assemblages in the lower part of the radiolarian-rich section of core can be considered different from the top part.

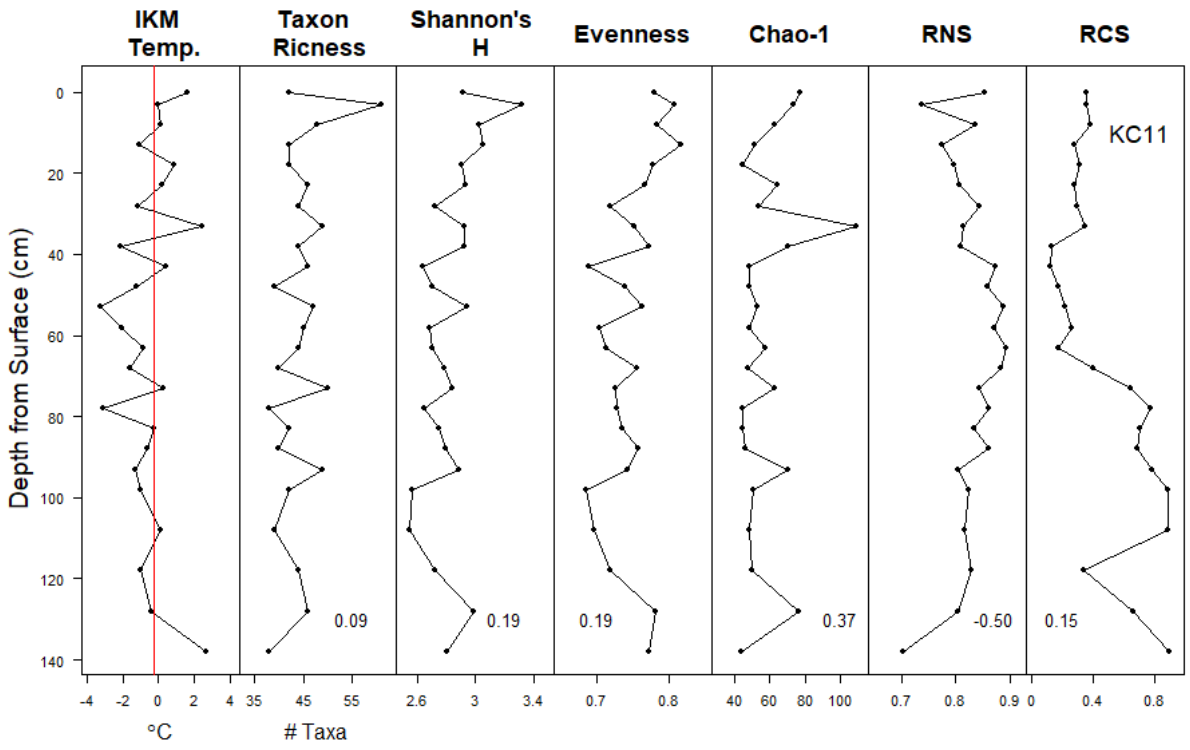

Figure 16: Palaeo-SSST estimates for KC11. Red line indicates the average modern SSST for the site. Diversity indices are plotted with Pearson's r values showing the correlation between the index and palaeo-SSST. Palaeo-SSST and RNS are significantly negatively correlated (r = -0.50, *p* = 0.01).

4.4 Discussion

4.4.1 SSST estimates

Using IKM, palaeo-SSST estimates were calculated for core top and box core samples with high enough radiolarian TA to derive assemblage data. The estimated modern SSST values the Sabrina Coast core tops were between 0.03 °C (KC08) and 3.3 °C (KC13) (S.E. ±1.97 °C). Core top palaeo-SSST estimations can be compared directly with the observed average SSST values for the corresponding sites. Palaeo-SSST for Two Sabrina Coast core tops (KC03 and KC13) were well overestimated with residuals of -3.2 °C and -3.1 °C respectively, the two largest residuals of the reference dataset. The reason for this is unclear. KC03 and KC13 were sorted into different clusters (Cluster 2 and Cluster 1 respectively), likely due to the difference in *Antarctissa* spp. RA (33.3% vs 24.4%), so do not have particularly similar assemblages. RA values for *S. aculeata/validispina*, the species which is most influential in F1, are also not unusual

in these samples. Geographically they do not have much in common. KC03 is the shallowest site (1862 m) and is the most westerly, located on a depositional ridge in Area A, while KC13 is one of the deeper sites (3321 m) and located in a canyon in Area C. They are, however, the core tops with the highest TA values (~40.5k and ~30k). It may be that there is lateral transportation of siliceous plankton to these sites accounting for the high TA values and the palaeo-SSST anomalies.

Palaeo-SSST estimates for box core samples ranged from -3.26 °C (KC11-53) to 3.26 °C (KC05-11). Given seawater has a freezing point of ~-2 °C, it is likely that temperature estimates much below this are underestimates of palaeo-SSST, particularly when standard error is considered.

Palaeo-SSST estimates do not change linearly through Termination I and the Holocene to the present day. There is no significant correlation with sample depth, and no difference in the mean palaeo-SSST of the three main clusters, which can be viewed as distinguishing the different 'stages' of the interglacial conditions of the Holocene (Clusters 1 and 2) from the more glacial conditions of Termination I (Cluster 3). Logically, cooler temperatures could be expected during Termination periods as the general state of the ocean moves from glacial, sea-ice covered to interglacial open ocean.

Controls on SSST such as the relationship of temperature with sea-ice, water column stratification and westerly wind patterns, should be further considered as per studies in other parts of the Southern Ocean (Menviel et al., 2008; Shevenell et al., 2011).

4.4.2 IKM procedure

While the IKM is an established method for reconstructing palaeoclimatic variables, some aspects of this study prevent palaeo-SSST estimates from being as accurate as they could be. The reference dataset contained only a small number of core tops which were representative of the conditions found at the study site (Fig. 13). With only 8 suitable core tops from the Sabrina Coast, and with these core tops being in close proximity of each other, it was necessary to expand the reference dataset by adding core top assemblage data from an external source. 47 core tops from the Cortese and Prebble (2015) modern analogue dataset were added to the reference dataset. Despite restricting these core tops to those that were further south than 45°S, they still covered a large temperature gradient with average modern SSST ranging from -1.12 °C – 18.49 °C. Based on temperature, the core tops in the reference dataset seemed

to fall into one of two groups, a warmer group with median average modern temperatures of ~14 °C and a cooler group with median average modern temperatures ~2 °C (Fig. 14). Besides temperature, other factors which control radiolarian assemblages differ greatly between the Sabrina Coast core tops and most of the reference dataset, e.g. seasonal sea-ice versus year-round open ocean, upwelling systems and differing vertical structure of the water column. The Sabrina Coast core tops are thermally, as well as, spatially distant from much of the reference dataset resulting in a high proportion of 'no analogue' values appearing in the IKM output as the box core assemblages differed quite radically from many of the reference dataset assemblages.

The 5 factors included in the IKM procedure account for ~92% of the variance in the reference dataset. Two factors would likely have been appropriate for palaeo-SSST calculations as together they account for ~78% of the variance in the reference dataset. However, due to the spatial and thermal range of the reference dataset it was decided that factors with less contribution to explaining the variance should be included – particularly as F5 was characterised by the contrast between the RA of *S. arachnea* (SVFS 2.73) and *C. davisiana* RA (SVFS -2.61), two species which were shown to play a large part in the cluster analysis and in differentiating Termination I from the interglacial. F1, the factor which accounts for the largest portion of the variance in the reference dataset, was influenced by *S. aculeata/validispina*, a species which had an average RA of 1.1% in samples from this study. It may be a concern that factor analysis of the reference dataset placed so much importance on a species with such a low RA in the box core samples.

Curating a core top dataset made up solely of samples located south of the Sub-Antarctic front, and incorporating samples west of Tasmania, and close to the sea-ice edge/continental shelf, may allow taxa which are more specialised to Southern Ocean conditions to have a larger influence in the factor loadings.

4.4.3 Palaeo-SSST and diversity

The abundance and diversity of radiolarian assemblages do not correlate with changes in estimated Holocene SSST. In both cores the only measure which had a strong relationship with palaeo-SSST was RNS. Higher temperature estimates coincide with lower RNS values, and vice versa. A lack of palaeo-SSST related change in radiolarian assemblages throughout Termination I and the interglacial may be

because the temperature range in these waters was not extreme enough to cause a significant shift in species abundance or composition. Two of the three most abundant taxa, *C. davisiana* and *S. arachnea,* are not endemic to the Southern Ocean. Their tolerance of a range of temperatures means their RA may not be affected by changes of only a few degrees Celsius in SSST, therefore explaining the lack of correlation between radiolarian diversity and palaeo-SSST. The differences between radiolarian assemblages which saw samples classified into distinct clusters may owe more to changes in water column properties, such as stratification vs vertical mixing, rather than to changes in temperature. Estimated palaeo-SSSTs calculated using a more specialised core top reference dataset may prove to have significant correlations with radiolarian diversity indices.

5. Conclusion

The Southern Ocean plays an important role in the global climate system but, despite this, there are regions for which the palaeoclimatic history is understudied. This study confirmed that fossil radiolarians are a useful proxy for reconstructing palaeoclimate in the Sabrina Coast region of East Antarctica. Radiolarians from two 2.5 m sediment cores, extracted from the Sabrina Coast continental slope, were identified and counted, with their abundance and composition used to make inferences about palaeoclimate of this region. High radiolarian and diatom abundance, and low magnetic susceptibility, were indicative of interglacial conditions, i.e. the Holocene, while the near absence of siliceous microfossils and higher, more variable, magnetic susceptibility indicated the glacial conditions. Foraminifera-based ^{14}C dating, and the relative abundance of the radiolarian species, *C. davisiana* were used to build an age model for core KC05. This confirmed that the known timing of the glacial/interglacial transition coincided with specific change/s in the total abundance of radiolarians. In addition, peaks in *C. davisiana* near the glacial/interglacial boundary indicated that during Termination I the water column may have been highly stratified with a low salinity surface layer overlying a warmer intermediate water mass. Holocene palaeotemperatures were estimated using the Imbrie-Kipp (1971) transfer function method using a reference set made up of Sabrina Coast core tops, plus samples from an existing Southern Hemisphere radiolarian core top dataset curated by Cortese and Prebble (2015). Overall this research found that radiolarians should be included alongside other proxy methods when reconstructing the palaeoclimate of the Sabrina

Coast region. Radiolarian total abundance is indicative of sea-ice versus open ocean conditions, *C. davisiana* can be used as a stratigraphic tool, as well as providing information about water column stratification, and assemblage data can be used to estimate past summer sea-surface temperature.

The research outlined in Section 3 showed that the radiolarian record in Sabrina Coast sediments, as far back as marine isotope stage 3, is both well preserved enough, and informative enough, to identify large scale climate events such as glacial/interglacial cycles, and the transition period between them. Cluster analysis was used to classify similar radiolarian assemblages into distinct clusters. Clusters 1 and 2, consisting of all eight Sabrina Coast core top samples, and samples which came mostly from the upper part of the cores, represent the interglacial conditions of the Holocene. Cluster 3 samples were restricted to the lower part of the radiolarian-rich section of the core, and represented Termination I. Foraminifera-based ^{14}C dates, and peaks in *C. davisiana* abundance, were used to construct three age models. The model based on Davisiana Event 2 matched best with the known timing of the boundaries between marine isotope stages 3/2, and 2/1. The age model helped verify that radiolarian abundance at this site was linked to glacial/interglacial cycles.

Future work is planned using other cores collected on IN2017-V01. Preliminary magnetic susceptibility and natural gamma data from six piston cores, between ~12 m and ~16 m in length, indicate they are likely to contain sediments from as far back as MIS10 (~330-370 ka) (Armand et al., 2018; Lisiecki and Raymo, 2005). These cores likely contain radiolarian assemblage data that span multiple glacial/interglacial cycles. Longer cores will allow for comparisons between assemblages not only from the same interglacial period, but from multiple interglacial periods. Identification of assemblages which are typical of the same stage during differing interglacial periods may be possible as well as pinpointing which environmental factors affect diversity and richness of radiolarian taxa. *Siphocampe arachnea* has the potential to be an important species in palaeoclimate reconstructions in this region with relative abundance that has a strong negative correlation with the relative abundance of *C. davisiana*. More research into the relation between the two species, both at this site and using other palaeo datasets, is warranted as it may prove a useful measure for climate reconstructions in this, and other, Southern Ocean regions.

Summer sea-surface palaeotemperature estimates were calculated using the Imbrie-Kipp (1971) transfer function method as outlined in Section 4. Palaeo-SSST's ranged

from -3.26 °C to 3.26 °C (standard error ±1.97 °C). SSST estimates towards the lower end of the range appear to be underestimating palaeo-SSST as it is not likely seawater would exist in a liquid state at such low temperatures. Palaeo-SSST did not have an influence on radiolarian diversity or richness and did not correlate with stratigraphic position in the core. The only diversity measure which temperature seemed to influence was the ratio of nassellarian to spumellarian taxa – the explanation for this is not yet known.

The reference dataset used for IKM could be substantially improved before making palaeo SSST estimates in future studies. The climatic conditions of the locations of the core tops included in the reference dataset were substantially different from the location of the study site, however, it has been shown that Sabrina Coast radiolarian assemblages were of a quality such that Palaeo-SSST estimates were successfully calculated using the IKM transfer function.

This study was a pilot study for a planned Ph.D. project. Having investigated the viability of using radiolarians as a climate proxy in this region, and identifying areas of improvement, longer cores, also collected on IN2017-V01, will be used for palaeoclimate reconstructions expected to span several glacial/interglacial cycles.

References

Abelmann, A., and Gersonde, R., 1991. Biosiliceous particle flux in the Southern Ocean. *Marine Chemistry*, 35(1), 503-536.

Abelmann, A., and Gowing, M. M., 1997. Spatial distribution pattern of living polycystine radiolarian taxa - baseline study for paleoenvironmental reconstructions in the Southern Ocean (Atlantic sector). *Marine Micropaleontology*, 30, 3-29.

Abelmann, A., Brathauer, U., Gersonde, R., Sieger, R., and Zielinski, U., 1999. Radiolarian-based transfer function for the estimation of sea surface temperatures in the Southern Ocean (Atlantic Sector). *Paleoceanography*, 14(3), 410-421.

Armand, L. K., Crosta, X., Romero, O., and Pichon, J.-J.,2005. The biogeography of major diatom taxa in Southern Ocean sediments: 1. Sea ice related species. *Palaeogeography, Palaeoclimatology, Palaeoecology*, 223(1), 93-126.

Armand, L.K, O'Brien, P.E. and On-board Scientific Party, 2018. *Interactions of the Totten Glacier with the Southern Ocean through multiple glacial cycles (IN2017-V01): Post-survey report*, Research School of Earth Sciences, Australian National University: Canberra

Azaneu, M., Kerr, R., Mata, M. M., and Garcia, C. A. E., 2013. Trends in the deep Southern Ocean (1958–2010): Implications for Antarctic Bottom Water properties and volume export. *Journal of Geophysical Research: Oceans*, 118(9), 4213-4227.

Benz, V., Esper, O., Gersonde, R., Lamy, F., and Tiedemann, R., 2016. Last Glacial Maximum sea surface temperature and sea-ice extent in the Pacific sector of the Southern Ocean. *Quaternary Science Reviews*, 146, 216-237.

Boltovskoy, D., 1994. The sedimentary record of pelagic biogeography. *Progress in Oceanography*, 34(2), 135-160.

Boltovskoy, D., and Correa, N., 2016. Biogeography of Radiolaria Polycystina (Protista) in the World Ocean. *Progress in Oceanography*, 149, 82-105.

Boltovskoy, D., Kling, S. A., Takahashi, K., and Bjorklund, K. R., 2010. World Atlas of Distribution of Recent Polycystina (Radiolaria). *Palaeontologia Electronica*, 13(3), 18A:230.

Caldeira, K., and Duffy, P. B., 2000. The Role of the Southern Ocean in Uptake and Storage of Anthropogenic Carbon Dioxide. *Science*, 287(5453), 620-622.

Cortese, G., and Abelmann, A., 2002. Radiolarian-based paleotemperatures during the last 160 kyr at ODP Site 1089 (Southern Ocean, Atlantic Sector). *Palaeogeography, Palaeoclimatology, Palaeoecology*, 182(3), 259-286.

Cortese, G., Abelmann, A., & Gersonde, R., 2007. The last five glacial-interglacial transitions: A high-resolution 450,000-year record from the subantarctic Atlantic. *Paleoceanography*, 22(4), PA4203.

Cortese, G., and Prebble, J., 2015. A radiolarian-based modern analogue dataset for palaeoenvironmental reconstructions in the southwest Pacific. *Marine Micropaleontology*, 118, 34-49.

Crosta, X., Sturm, A., Armand, L., and Pichon, J.-J., 2004. Late Quaternary sea ice history in the Indian sector of the Southern Ocean as recorded by diatom assemblages. *Marine Micropaleontology*, 50(3), 209-223.

Dowsett, H. J., 2009. Foraminifera. In V. Gornitz (editor), *Encyclopedia of Paleoclimatology and Ancient Environments*. Dordrecht: Springer Netherlands. 338-339.

Fengming, C., Tiegang, L., Lihua, Z., & Jun, Y., 2008. A Holocene paleotemperature record based on radiolaria from the northern Okinawa Trough (East China Sea). *Quaternary International*, 183(1), 115-122.

Galili, T., 2015. dendextend: an R package for visualizing, adjusting, and comparing trees of hierarchical clustering. Bioinformatics.

Gersonde, R., Crosta, X., Abelmann, A., and Armand, L., 2005. Sea-surface temperature and sea ice distribution of the Southern Ocean at the EPILOG Last Glacial Maximum—a circum-Antarctic view based on siliceous microfossil records. *Quaternary Science Reviews*, 24(7), 869-896.

Greenbaum, J. S., Blankenship, D. D., Young, D. A., Richter, T. G., Roberts, J. L., Aitken, A. R. A., Legresy, B., Schroeder, D. M., Warner, R. C. van Ommen, T. D. and Siegert, M. J., 2015. Ocean access to a cavity beneath Totten Glacier in East Antarctica. *Nature Geoscience*, 8, 294.

Guiot, J., and de Vernal, A., 2007. Transfer Functions: Methods for Quantitative Paleoceanography Based on Microfossils. In C. Hillaire-Marcel and A. de Vernal (editors), *Developments in Marine Geology: Proxies in Late Cenozoic Paleoceanography (Vol. 1)*. London: Elsevier.

Gupta, S. M., & Malmgren, B. A., 2009. Comparison of the accuracy of SST estimates by artificial neural networks (ANN) and other quantitative methods using radiolarian data from the Antarctic and Pacific Oceans. *Earth Science India*, 2(2), 52-75.

Gwyther, D. E., Galton-Fenzi, B., Hunter, J. R., and Roberts, J. L., 2014. Simulated melt rates for the Totten and Dalton ice shelves. *Ocean Science*, 10(3), 267.

Hammer, O., Harper, D. A. T., and Ryan, P. D., 2001. Paleontological Statistics Software Package for Education and Data Analysis. *Palaeontologia Electronica*, 4(1), 9.

Hays, J. D., Imbrie, J., and Shackleton, N. J., 1976. Variations in the Earth's orbit: pacemaker of the ice ages. *Science*, 194(4270), 1121-1132.

Hernández-Almeida, I., Cortese, G., Yu, P. S., Chen, M. T., & Kucera, M., 2017. Environmental determinants of radiolarian assemblages in the western Pacific since the last deglaciation. *Paleoceanography*, 32.

Imbrie, J., and Kipp, N. G., 1971. A new micropaleontological method for quantitative paleoclimatology: Application to a late Pleistocene Caribbean core. In K. K. Turekian (editor), *The Late Cenozoic Glacial Ages*. New Haven, Connecticut: Yale University Press. 71-181.

Knoll, A., and Kotrc, B., 2015. Protistan Skeletons: A Geologic History of Evolution and Constraint. In C. Hamm (editor), *Evolution of lightweight structures: Analyses and Technical Applications*. Dordrecht: Springer Science+Business Media.

Kotrys, B., 2014. Paleotemperature reconstruction at the Polar Front in the Southern Ocean (Atlantic sector) based on the middle-upper Pleistocene radiolarian record from ODP Leg 177 Site 1091. *Przeglad Geologiczny*, 62(9), 448-455.

Krabberød, A., K., , Bråte, J., Dolven, J. K., Ose, R. F., Klaveness, D., Kristensen, T., Bjørklund, K.,R. and Shalchian-Tabrizi, K., 2011. Radiolaria Divided into Polycystina and Spasmaria in Combined 18S and 28S rDNA Phylogeny. *PLoS One*, 6(8).

Kruglikova, S. B., Bjorklund, K. R., Dolven, J. K., Hammer, O., and Cortese, G., 2010. High-rank polycystine radiolarian taxa as temperature proxies in the Nordic Seas. *Stratigraphy*, 7(4), 265-281.

Kucera, M., 2015. Modern analogue techniques. In J. Harff, M. Meschede, S. Petersen and J. Thiede (editors), *Encyclopedia of Marine Geosciences*.. Dordrecht: Springer Science+Business Media.

Labracherie, M., Labeyrie, L. D., Duprat, J., Bard, E., Arnold, M., Pichon, J.-J., and Duplessy, J.-C., 1989. The Last Deglaciation in the Southern Ocean. *Paleoceanography*, 4(6), 629-638.

Lamy, F., Kilian, R., Arz, H. W., Francois, J.-P., Kaiser, J., Prange, M., and Steinke, T., 2010. Holocene changes in the position and intensity of the southern westerly wind belt. *Nature Geoscience*, 3, 695.

Lazarus, D. B., Suzuki, N., Caulet, J.-P., Nigrini, C., Goll, I., Goll, R., Dolven, J.K. Diver, P. and Sanfilippo, A., 2015. An evaluated list of Cenozic-Recent radiolarian species names (Polycystinea), based on those used in the DSDP, ODP and IODP deep-sea drilling programs. *Zootaxa*, 3999(3), 310-333.

Le Quere, L., Rödenbeck, C., Buitenhuis, E.T., Conway, T.J., Langenfelds, R., Gomez, A., Labuschagne, C., Ramonet, M., Nakazawa, T., Matzl, N., Gillett, N. and Heimann, M., 2007. Saturation of the Southern Ocean CO2 Sink Due to Recent Climate Change. *Science*, 316,1735-1737.

Leventer, A., 2009. Diatoms. In V. Gornitz (editor), *Encyclopedia of Paleoclimatology and Ancient Environments* (pp. 279-280). Dordrecht: Springer Netherlands.

Lisiecki, L. E., and Raymo, M. E., 2005. A Pliocene-Pleistocene stack of 57 globally distributed benthic δ18O records. *Paleoceanography*, 20(1).

Locarnini, R. A., Mishonov, A. V., Antonov, J. I., Boyer, T. P., Garcia, H. E., Baranova, O. K., Zweng, M.M., Paver, C.R., Reagan, J.R., Johnson, D.R., Hamilton and M. Seidov, D., 2013. World Ocean Atlas 2013. In S. Levitus and A. Mishonov (editors), *Volume 1: Temperature*.

Lozano, J. A., & Hays, J. D., 1976. Relationship of radiolarian assemblages to sediment types and physical oceanography in the Atlantic and western Indian Ocean sectors of the Antarctic Ocean. In *Investigation of Late Quaternary Paleoceanography and Paleoclimatology* (Vol. 145, pp. 303-336). Geological Society of America Boulder, CO.

Lüer, V., Cortese, G., Neil, H. L., Hollis, C. J., & Willems, H., 2009. Radiolarian-based sea surface temperatures and paleoceanographic changes during the Late Pleistocene–Holocene in the subantarctic southwest Pacific. *Marine Micropaleontology*, 70(3–4), 151-165.

Masson-Delmotte, V., M., S., Abe-Ouchi, A., Beer, J., Ganopolski, A., González Rouco, J. F., Jansen, E., Lambeck, K., Luterbacher, J., Naish, T., Osborn, T., Otto-Bliesner, B., Quinn, T., Ramesh, R., Rojas, M., Shao, X., and Timmermann, A., 2013. Information from Paleoclimate Archives. In T. F. Stocker, D. D. Qin, G.-K. Plattner, M. Tignor, S. K. Allen, J. Boschung, A. Nauels, Y. Xia, V. Bex, and P. M. Midgley (editors), *Climate Change 2013: The Physical Science Basis. Contribution of Working Group I to the Fifth Assessment Report of the Intergovernmental Panel on Climate Chan*ge. Cambridge, United Kingdom and New York, NY, USA: Cambridge University Press.

Matsuzaki, K. M., Nishi, H., Suzuki, N., Kawate, Y., Takashima, R., and Sakai, T., 2014. *Cycladophora davisiana* abundances as a paleoceanographic and

stratigraphic tool in high latitude siliciceous sediments. *Marine Micropaleontology*, 106, 1-9.
Matsuzaki, K. M., and Itaki, T., 2017. New northwest Pacific radiolarian data as a tool to estimate past sea surface and intermediate water temperatures. *Paleoceanography,* 32(3), 2017PA003087.
Matul, A. G., 2011. The recent and quaternary distribution of the radiolarian species *Cycladophora davisiana*: A biostratigraphic and paleoceanographic tool. *Oceanology,* 51(2), 335-346.
Menviel, L., Timmerman, A., Mouchet, A. and Timm, O., 2008. Climate and marine carbon cycle response to changes in the strength of the Southern Hemispheric westerlies, *Paleoceanography*, 23, PA4201.
Morley, J. J., & Hays, J. D., 1979. *Cycladophora davisiana*: a stratigraphic tool for Pleistocene North Atlantic and interhemispheric correlation. *Earth and Planetary Science Letters*, 44(3), 383-389.
Morley, J. J., and Hays, J. D., 1983. Oceanographic conditions associated with high abundances of the radiolarian *Cycladophora davisiana*. *Earth and Planetary Science Letters*, 66, 63-72.
Niebler, H. S., and Gersonde, R., 1998. A planktic foraminiferal transfer function for the southern South Atlantic Ocean. *Marine Micropaleontolog*y, 34(3), 213-234.
Nishimura A, and Nakaseko, K., 2011. Characterization of radiolarian assemblages in the surface sediments of the Antarctic Ocean. *Palaeoworld*, 20(2), 232-251.
Oksanen, J., Blanchet, F.G., Friendly, M., Kindt, R., Legendre, P., McGlinn, D., Minchin, P.R., O'Hara, R. B., Simpson, G.L., Solymos, P., Stevens, M.H.M., Szoecs, E., and Wagner, H., 2018. vegan: Community Ecology Package. R package version 2.5-2. <CRAN.R-project.org/package=vegan>
Panitz, S., Cortese, G., Neil, H. L., & Diekmann, B., 2015. A radiolarian-based palaeoclimate history of Core Y9 (Northeast of Campbell Plateau, New Zealand) for the last 160 kyr. *Marine Micropaleontology*, 116(Supplement C), 1-14.
Perera, R., 2017. Honours Thesis, Australian National University, Canberra, Australia.
Petrushevskaya, M. G., 1967. Radiolyarii otryadov Spumellariai Nassellaria Antarkticheskoi oblasti (po materialam Sovetskoi Antarkticheskikh ekspeditsii). Rezultaty Biologicheskikh Issledovanii Sovetskoi Antarkticheskoi Ekspeditsii 1955-1958, 3, 5-186.
Pichon, J. J., Labracherie, M., Labeyrie, L. D., and Duprat, J., 1987. Transfer functions between diatom assemblages and surface hydrology in the southern ocean. *Palaeogeography, Palaeoclimatology, Palaeoecology*, 61, 79-95.
R Core Team, 2018. R: A language and environment for statistical computing. R Foundation for Statistical Computing, Vienna, Austria. <www.R-project.org/>.
radiolaria.org, 2018. *radiolaria.org*, < http://www.radiolaria.org/>
Richter, C., Acton, G., Endris, C., and Radsted, M., 2007. Handbook for Shipboard Paleomagnetists. *ODP Tech. Note*, 34.
Rignot, E., Jacobs, S., Mouginot, J., and Scheuchl, B., 2013. Ice-Shelf Melting Around Antarctica. *Science*, 341(6143), 266-270. doi:10.1126/science.1235798
Roberts, J., Galton-Fenzi, B. K., Paolo, F. S., Donnelly, C., Gwyther, D. E., Padman, L., Young, D., Warner, R., Greenbaum, J., Fricker, H. A., Payne, A. J., Cornford, S., Le Brocq, A., van Ommen, T., Blankenship, D., and Siegert, M. J., 2017. Ocean forced variability of Totten Glacier mass loss. *Geological Society, London, Special Publications*, 461.
Robertson, J.H., 1975. Thesis, Columbia University.

Rogers, J., & De Deckker, P., 2007. Radiolaria as a reflection of environmental conditions in the eastern and southern sectors of the Indian Ocean: A new statistical approach. *Marine Micropaleontology*, 65(3), 137-162.

Rogers, J., and De Deckker, P., 2011. Environmental reconstructions of the upper 500 m of the southern Indian Ocean over the last 40 ka using Radiolarian (Protista) proxies. *Quaternary Science Reviews,* 30(7), 876-886.

Saraswati, P. K., and Srinivasan, M. S., 2016. *Micropaleontology: Principles and Applications*. Switzerland: Springer International Publishing.

Schlitzer, R., 2002. Interactive analysis and visualization of geoscience data with Ocean Data View. *Computers & Geosciences*, 28, 1211-1218.

Shevenell, A. E., Ingalls, A. E., Domack, E. W., and Kelly, C., 2011. Holocene Southern Ocean surface temperature variability west of the Antarctic Peninsula. *Nature*, 470, 250.

Sieger, R., Gersonde, R., and Zielinski, U., 1999. New software package available for quantitative paleoenvironmental reconstructions. *Eos, Transactions American Geophysical Union*, 80(19)

Suzuki, N., and Aita, Y., 2011. Radiolaria: achievements and unresolved issues: taxonomy and cytology. *Plankton and Benthos Research*, 6(2), 69-91.

Suzuki, N., and Not, F., 2015. Biology and Ecology of Radiolaria. In S. Ohtsuka, T. Suzaki, T. Horiguchi, N. Suzuki, and F. Not (editors), *Marine Protists: Diversity and Dynamics*. Japan: Springer.

Tabachnick, B. G., and Fidell, L. S., 2013. *Using Multivariate Statistics (6 ed.)*. USA: Pearson.

Takahashi, K., 1991. Radiolaria: flux, ecology, and taxonomy in the Pacific and Atlantic. In S. Honjo (editor), *Ocean Biocoenosis Series 303*. Woods Hole, MA: Woods Hole Oceanographic Institution.

van Tongeren, O. F. R., 1995. Cluster Analysis. In R. H. G. Jongman, C. J. F. ter Braak, and O. F. R. van Tongeren (editors), *Data analysis in community and landscape ecology (2 ed.)*. Cambridge, UK: Cambridge University Press.

WoRMS Editorial Board, 2018. World Register of Marine Species. Available from http://www.marinespecies.org at VLIZ.

Yasudomi, Y., Motoyama, I., Oba, T., & Anma, R., 2014. Environmental fluctuations in the northwestern Pacific Ocean during the last interglacial period: Evidence from radiolarian assemblages. *Marine Micropaleontology*, 108(Supplement C), 1-12.

Zielinski, U., and Gersonde, R., 1997. Diatom distribution in Southern Ocean surface sediments (Atlantic sector): Implications for paleoenvironmental reconstructions. *Palaeogeography, Palaeoclimatology, Palaeoecology*, 129(3), 213-250.

Supplementary Material

Supplement A: List of radiolarian taxa counted for this study. Raw datasets will be made available online via the Marine National Facility as is required.

Nassellaria

Actinommidae	
Actinomma	Haeckel 1860
Actinomma antarcticum	(Haeckel) Nigrini 1967
Actinomma boreale	Cleve 1899
Actinomma delicatulum	(Dogiel) in Dogiel and Reshetnyak 1952
Actinomma kergeulenis	Caulet 1991
Actinomma leptoderma longispina	Cortese and Bjørklund 1998
Actinomma leptodermum	(Jørgensen) Nigrini and Moore 1979
Actinomma trinacria	(Haeckel) Cortese and Bjørklund 1998
Cenosphaera	Ehrenberg 1854
Cenosphaera cristata	Haeckel 1887
Druppatractus	Haeckel 1887
Druppatractus ostracion	Haeckel, 1887
Druppatractus variabilis	Dumitrica 1973
Gonosphaera	Jørgensen 1905
Gonosphaera primordialis	Jørgensen 1905
Lonchosphaera	Popofsky 1908
Lonchosphaera spicata	Popofsky 1908
Rhizoplegma	Haeckel 1881
Rhizoplegma boreale	Popofsky 1908
Sphaeropyle	Dreyer 1889
Sphaeropyle antarctica	(Dreyer) 1880
Stylatractus	Haeckel 1887
Stylatractus neptunus	Haeckel 1887
Styptosphaera	Haeckel 1881
Styptosphaera spumacea	Haeckel 1887
Litheliidae	
Discopyle	Haeckel 1887
Larcopyle buetschlii	Dreyer 1889
Larcopyle pylomaticus	(Riedel) Lazarus et al. 2005
Larcopyle weddellium	Lazarus et al. 2005
Lithelius	Haeckel 1860
Lithelius minor	Jørgensen 1900
Lithelius nautiloides	Popofsky 1908
Pyloniidae	
Dipylissa	Dumitrica 1988
Dipylissa bensoni	Dumitrica 1988
Hexapyle	Haeckel 1881
Hexapyle dodecantha	Haeckel 1887
Phorticium	Haeckel 1881
Phorticium clevei	(Jørgensen) Petrushevskaya 1967
Spongodiscidae	
Spongodiscus	Ehrenberg 1854
Spongodiscus resurgens	Ehrenberg 1854
Spongopyle	Dreyer 1889
Spongopyle osculosa	Dreyer 1889
Spongotrochus	Haeckel 1860
Spongotrochus glacialis	Popofsky 1908
Stylodictya	Ehrenberg 1847
Stylodictya aculeata	Jørgensen 1905
Stylodictya tenuispina	Jørgensen 1905
Stylodictya validispina	Jørgensen 1905
Tholoniidae	
Cubotholus	Haeckel 1887

Spumellaria

Artostrobiidae	
Botryostrobus	Haeckel 1887
Botryostrobus auritus-australis	Ehrenberg 1844
Siphocampe	Haeckel 1881
Siphocampe arachnea	(Ehrenberg) Nigrini 1977
Cannobotryidae	
Botryopyle	Haeckel 1881
Botryopyle cribrosa	(Ehrenberg) Haeckel 1887
Saccospyris	Haecker 1907
Saccospyris antarctica	Haecker 1907
Saccospyris conithorax	Petrushevskaya 1965
Saccospyris preantarctica	Petrushevskaya 1975
Carpocaniidae	
Carpocanarium	Haeckel 1887
Carpocanarium papillosum	(Ehrenberg) 1872
Collosphaeridae	
Acrosphaera	Haeckel 1881
Acrosphaera mercurius	Lazarus 1992
Plagiacanthidae	
Antarctissa	Petrushevskaya 1967
Antarctissa cylindrica	Petrushevskaya 1975
Antarctissa denticulata	Petrushevskaya 1967
Antarctissa strelkovi	Petrushevskaya 1967
Ceratocyrtis	Bütschli 1882
Ceratocyrtis histricosa	(Jørgensen) Petrushevskaya 1971
Cladoscenium	Haeckel 1881
Cladoscenium ancoratum	Haeckel 1887
Cladoscenium limbatum	Jørgensen 1905
Cladoscenium tricolpium	(Haeckel) Jørgensen 1900
Enneaphormis	Haeckel 1881
Enneaphormis rotula	Haeckel 1887
Lithomelissa	Ehrenberg 1847
Lithomelissa borealis	(Ehrenberg) Petrushevskaya 1967
Lithomelissa hystrix	Jørgensen 1900
Lithomelissa sp. A	Petrushevskaya 1967
Lithomelissa thoracites	Haeckel 1860
Lophophaena	Ehrenberg 1847
Lophophaena clevei	Petrushevskaya 1971
Mitrocalpis	Haeckel 1881
Mitrocalpis araneafera	(Ehrenberg) 1873
Peridium	Jørgensen 1900
Peridium longispinum	Haeckel 1887
Phormacantha	Jørgensen 1905
Phormacantha hystrix	(Jørgensen) Jørgensen 1905
Plectacantha	Jørgensen 1905
Protoscenium	Jørgensen 1905
Protoscenium simplex	Jørgensen 1905
Pseudodictyophimus	Petrushevskaya 1971
Pseudodictyophimus gracilipes	Caulet 1979
Pseudodictyophimus gracilipes multispinus	Bernstein 1934
Pseudodictyophimus platycephalus	(Haeckel) 1887
Tetraphormis	Haeckel 1881
Tetraphormis dodecaster	(Haeckel) Takahashi 1991
Theoperidae	
Artophormis	Haeckel 1881
Artophormis gracilis	Riedel 1959
Artostrobus	Haeckel 1887
Artostrobus annulatus	(Bailey) Haeckel 1887
Artostrobus Jørgenseni	Petrushevskaya 1967
Cornutella	Ehrenberg 1838
Cornutella profunda	Ehrenberg 1856
Cycladophora	Ehrenberg 1847
Cycladophora bicornis	(Popofsky) Lombari and Lazarus 1988
Cycladophora davisiana	Ehrenberg 1861
Cycladophora davisiana cornutoides	Petrushevskaya 1967
Cyrtolagena	Haeckel 1887
Cyrtolagena laguncula	Haeckel 1887
Dictyophimus	Ehrenberg 1847
Dictyophimus crisiae	Ehrenberg 1854
Dictyophimus hirundo	(Haeckel) Petrushevskaya 1975
Eucyrtidium	Ehrenberg 1847
Eucyrtidium annulatum	(Popofsky) 1913
Eucyrtidium teuscheri	Haeckel 1887
Gondwanaria	Petrushevskaya and Kozlova 1975
Gondwanaria campanulaeformis	(Campbell and Clark) 1945
Gondwanaria reshetnjakae	(Petrushevskaya) Petrushevskaya and Kozlova 1979

Spumellaria cont.

Litharachnium	Haeckel 1860	***Lophospyris***	Haeckel 1881
Litharachnium tentorium	Haeckel 1860	*Lophospyris pentagona quadriforis*	(Haeckel) 1887
Peripyramis	Haeckel 1881	***Tholospyris***	Haeckel 1881
Peripyramis circumtexta	Haeckel 1887	*Tholospyris gephyristes*	Huelsemann 1963
Sethoconus	Haeckel 1887	***Triceraspyris***	Haeckel 1881
Sethoconus tabulatus	Haeckel 1887	*Triceraspyris antarctica*	(Haecker) Haecker 1908
Trissocyclidae		***Zygocircus***	Bütschli 1882
Acanthodesmia	Mueller 1857	*Zygocircus productus*	(Hertwig) Haeckel 1887
Acanthodesmia micropora	(Popofsky) Petrushevskaya 1971		

Supplement B: Radiolarian taxa included in IKM palaeo-SSST estimates

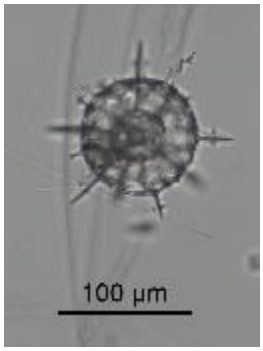

Actinomma boreale

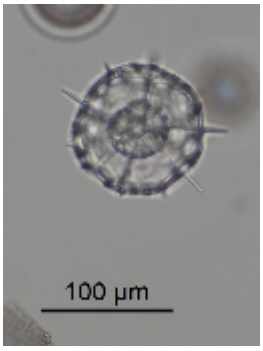

Actinomma leptodermum

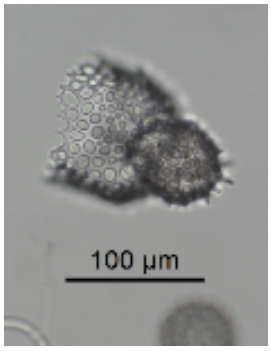

Antarctissa spp.

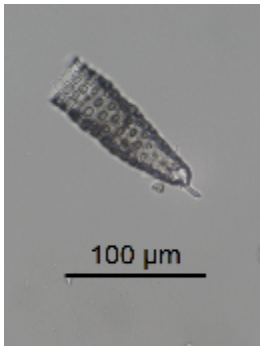

Artostrobus annulatus

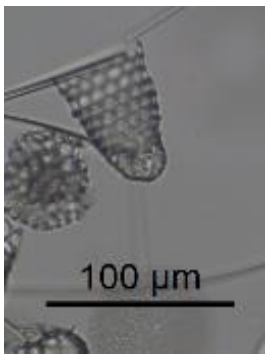

Artostrobus joergenseni

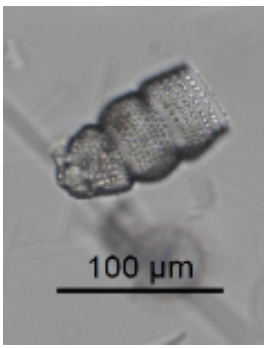

Botryostrobus auritus/australis

Cladoscenium anchoratum

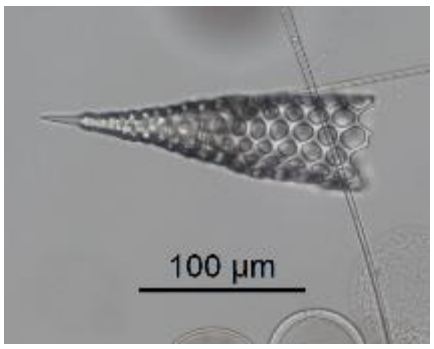

Cornutella profunda

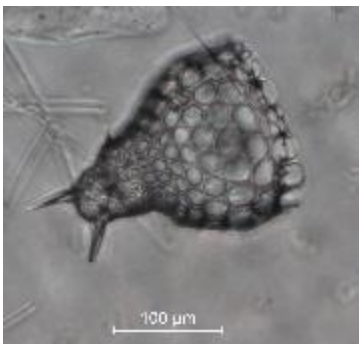

Cycladophora bicornis

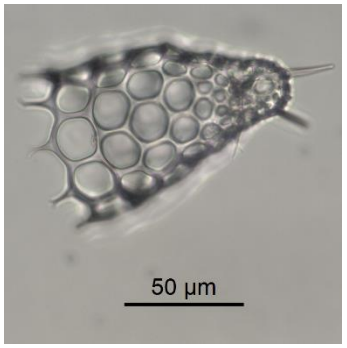

Cycladophora davisiana cornutoides

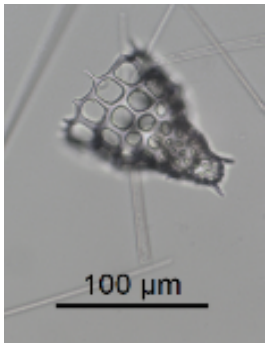

Cycladophora davisiana davisiana

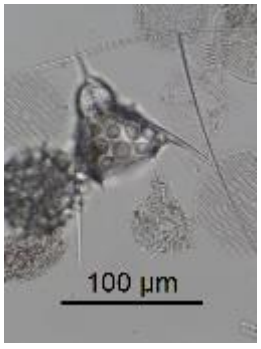

Dictyophimus crisae/hirundo

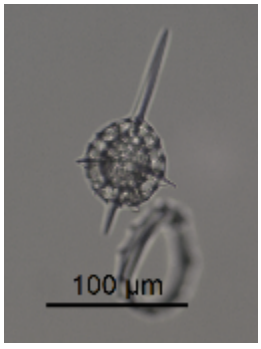

Druppatractus variabilis/ostracion

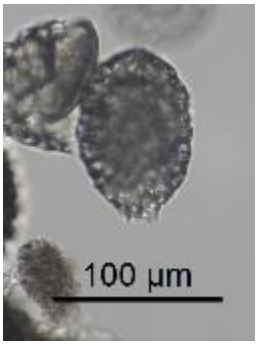

Larcopyle buetschlii

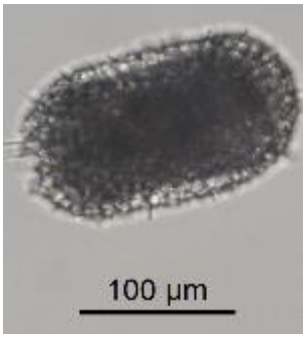

Larcopyle pylomaticus

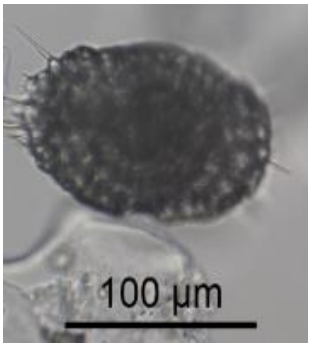

Larcopyle weddellium

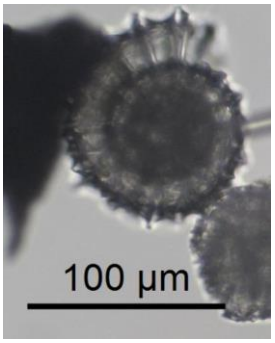

Lithelius nautiloides

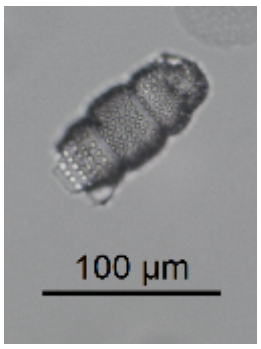

Lithocampe platycephala

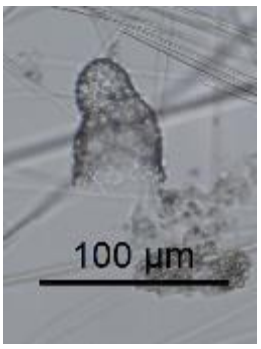

Lithomelissa boreale gr.

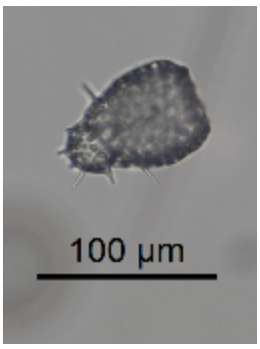

Lithomelissa sp. A

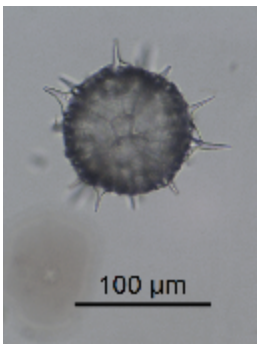

Loncosphaera spicata

Peridium longispinum

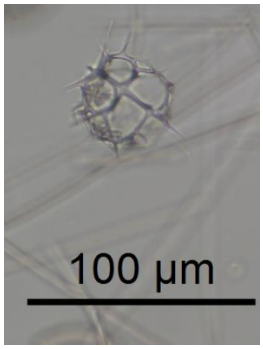

Phormacantha hystrix

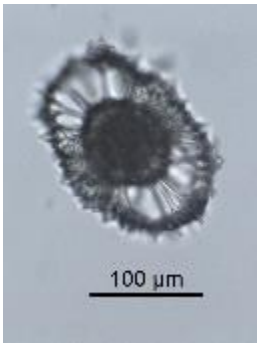

Phorticium clevei

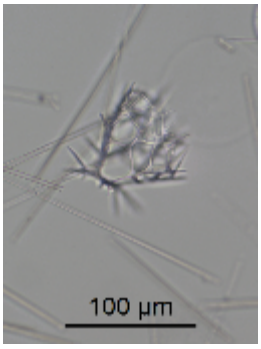

Plectacantha sp.

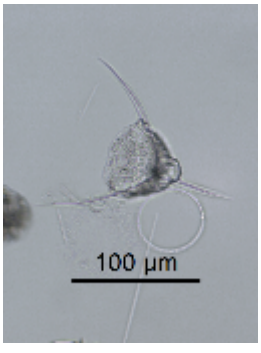

Pseudodictyophimus gracilipes s.l.

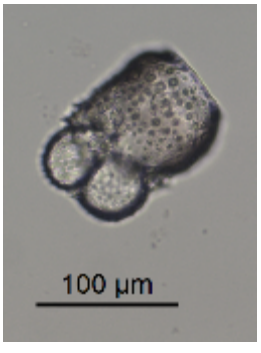

Saccospyris antarctica

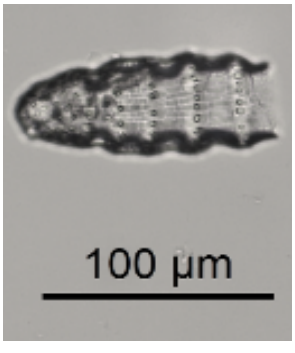

Siphocampe arachnea

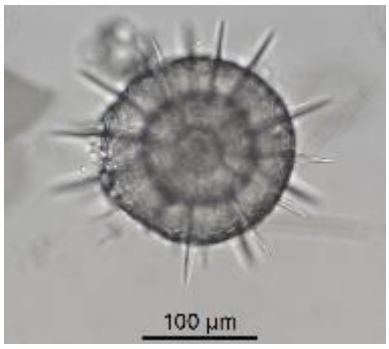

Sphaeropyle antarctica

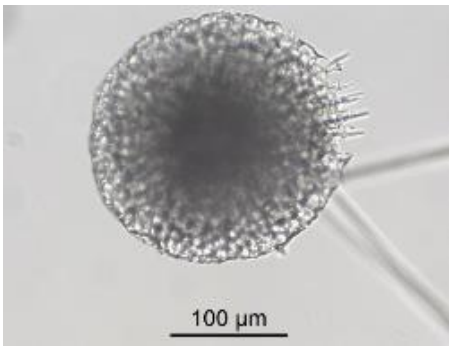

Spongotrochus osculosa/resurgens

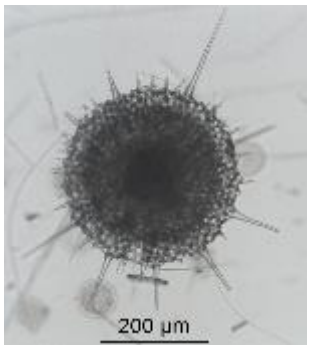

Spongotrochus glacialis

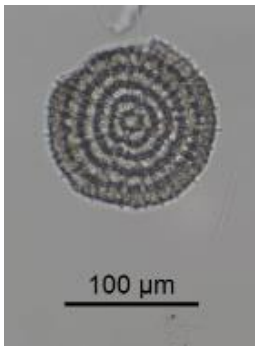

Stylodictya aculeata/validispina

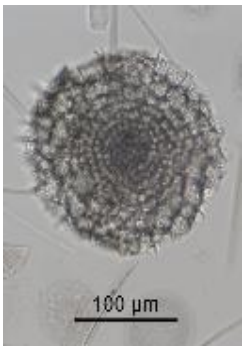

Stylodictya tenuispina

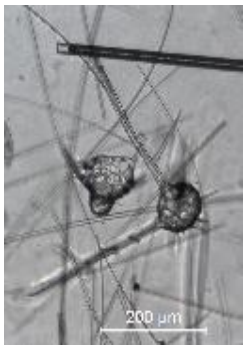

Tholospyris gephyristes (right)

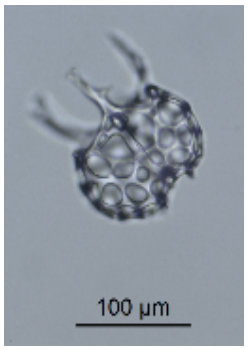

Triceraspyris antarctica

Supplement C: Canonical correspondence analysis (CCA) of all samples included in the cluster analysis i.e. the radiolarian-rich sections of KC05, KC11 and all Sabrina Coast core tops excluding KC07 due to low radiolarian abundance. The CCA result supports the classification of the samples into four clusters (Section 3.3.3, Figure 8). Clusters 1 and 2, and Cluster 3 are distinct from one another due to the relative abundance of *Cycladophora davisiana* (CA1) and represent the Holocene and Termination I stages. *Cycladophora davisiana* relative abundance is inversely correlated with CA1 scores placing the lone sample in Cluster 4 well away from the rest of the samples. CA1 accounts for 21% of the variance in the in dataset and CA2 accounts for 8% of the variance.

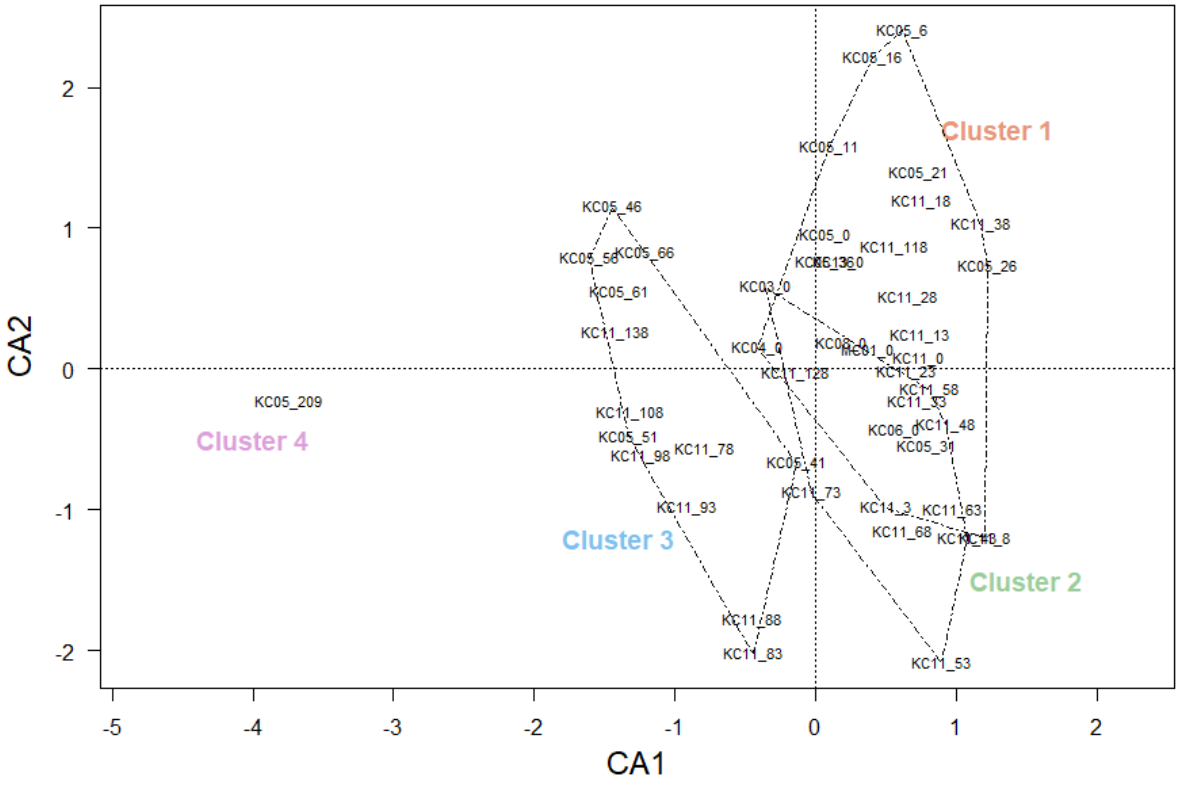

Supplement D: Statistical techniques used to reconstruct sea-surface temperature based on fossil radiolarian data in papers published between 2007 - 2017. Use of the Imbrie-Kipp transfer function method (IKM), modern analogue technique (MAT) and artificial neural networks (ANN) were specifically noted. Other techniques include the use of indicator species and weighted averaging-partial least squares regression.

Author/s	Year	IKM	MAT	ANN	Other
Rogers and De Deckker	2007		X		X
Cortese, Abelmann and Gersonde	2007	X			
Fengming et al.	2008	X			
Gupta and Malmgren*	2009	X	X	X	X
Luer et al.	2009	X			
Kruglikova et al.	2010	X			
Rogers and De Deckker	2011				X
Yasudomi et al.	2014				X
Matsuzaki et al.	2014				X
Kotrys	2014	X		X	
Panitz et al.	2015	X	X		
Cortese and Prebble	2015	X			
Hernandez-Almedia et al.	2017	X	X		X
Matsuzaki and Itaki	2017	X			

* This paper compared methods including Imbrie-Kipp transfer functions (IKM), the modern analogue technique (MAT), artificial neural networks (ANN), weighted-averaging partial least squares regression and the maximum likelihood method.

Supplement E: Scaled varimax factor scores for all taxa included in IKM. Values with an absolute value greater than 2 are bold indicating the corresponding taxon is important to the assemblage/factor.

Taxon	F1	F2	F3	F4	F5
Actinomma boreale	-0.111	0.061	0.537	0.202	-0.234
Actinomma leptodermum s.l.	0.602	-0.11	0.767	1.785	0.251
Antarctissa spp.	-0.07	**5.479**	-0.777	-0.227	-0.514
Artostrobus annulatus	-0.038	0.392	0.27	-0.145	0.911
Artostrobus joergenseni	0.02	0.14	0.318	-0.15	0.065
Botryostrobus auritus-australis	0.267	0.081	**3.734**	-0.268	0.354
Cladoscenium ancoratum	-0.008	0.048	0.013	-0.028	-0.034
Cornutella profunda	0.457	0.09	1.955	-0.331	-0.446
Cycladophora bicornis	0.091	0.399	1.068	0.389	0.865
Cycladophora davisiana cornutoides	0.029	0.084	0.131	0.017	0.01
Cycladophora davisiana davisiana	-0.095	1.078	0.499	0.228	**-2.612**
Dictyophimus crisiae/hirundo	0.128	0.061	0.457	-0.106	-0.653
Druppatractus variabilis/ostracion	0.018	0.227	0.312	-0.234	-0.156
Larcopyle butschlii	-0.019	0.103	1.696	-0.061	0.105
Larcopyle pylomaticus	-0.01	0.08	0.086	0.13	-0.146
Larcopyle weddellium	0.188	0.36	**2.347**	-0.679	-0.93
Lithelius nautiloides	-0.009	0.117	-0.016	-0.026	-0.005
Lithocampe platycephala	-0.067	0.237	0.362	-0.121	0.078
Lithomelissa boreale gr.	0.039	0.437	0.338	**2.426**	**2.859**
Lithomelissa sp. A	0.022	0.81	0.001	-0.195	1.222
Lonchosphaera spicata	-0.008	0.067	0.005	-0.045	-0.057
Peridium longispinum	-0.046	0.228	0.755	-0.3	0.17
Phormacantha spp.	-0.041	0.138	0.178	-0.088	-0.009
Phorticium clevei	0.186	0.157	-0.479	**2.137**	-1.936
Plectacantha sp.	-0.014	0.014	0.051	0.039	0.009
Pseudodictyophimus gracilipes s.l.	-0.159	0.526	1.519	1.104	0.025
Saccospyris antarctica	-0.071	0.502	0.034	0.375	-0.186
Siphocampe arachnea	0.099	1.258	0.455	-0.583	**2.726**
Sphaeropyle antarctica	-0.007	0.047	0.009	-0.026	-0.025
Spongopyle osculosa/resurgens	1.23	0.042	-0.026	**3.907**	0.042
Spongotrochus glacialis	0.149	0.119	0.202	1.422	-1.466
Stylodictya aculeata/validispina	**5.623**	0.026	-0.217	-1.055	-0.213
Stylodictya tenuispina	1.013	0.133	-1.299	-0.045	1.158
Tholospyris gephyristes	0.056	0.032	0.306	-0.182	0.052
Triceraspyris antarctica	0.023	0.274	-0.074	0.008	0.278

Supplement F: Example of R code. All R code used in this study was written by Kelly-Anne Lawler.

```
##Cluster analysis and Figure 8 ##

##Full analysis dataset - i.e. nothing excluded due to
percentages##

##Bray Curtis distance##

##Linkages - comp = complete (furthest neighbour)##

##Load cluster dataset##

setwd("~/MQ/MRes/2018/Datasets/Cluster")

Analysis_0p<-read.csv("Cluster_0p.csv", row.names=1,
check.names = TRUE)

##Transpose cluster dataset##

Analysis_0pT<-t(Analysis_0p)

##Load packages##

library(vegan)

library(dendextend)

##calculate distance measure (d) - default is bray-curtis##

d<-vegdist(Analysis_0pT)

##Also tried Jaccard distance NOTE: gives same clusters as
Bray-Curtis##

dJ<-vegdist(Analysis_0pT,method = "jaccard")

##cluster using furthest neighbour##

ccomp <- hclust(d, method="complete")

ccomp

##plot HORIZONTAL dendrogram, hang -1so that clusters all line
up at bottom##

dend<-as.dendrogram(ccomp)

##Colour branches per cluster membership##

d1=color_branches(dend,k=4, col = c("darksalmon",
"darkseagreen3","plum", "skyblue2"))

##Get list of sites and clusters they belong to##

cl <- cutree(ccomp, 4)

cl
```

```
##Add cluster membership to dataframe - Analysis dataset
becomes Cluster dataset##

Cluster_0pT<-cbind(Analysis_0pT,cl)

##Stacked bar charts of key species per site, started with Top
5, became Top 3##

Top5<-c("Antarctissa_spp.",
"Cycladophora_davisiana_davisiana", "Siphocampe_arachnea")

Analysis_0pT_Top5<-Analysis_0pT[,Top5]

Stacked<-transform(Analysis_0pT_Top5, Other=60-
rowSums(Analysis_0pT_Top5))

StackedT<-t(Stacked)

##Order bar chart by position on dendrogram##

clusterorder<-c("KC11_128",  "KC04_0", "KC05_0", "KC06_0",
"KC11_33", "KC13_0", "KC05_36", "KC11_118", "KC05_6",
"KC05_16", "KC05_21", "KC05_26", "KC11_28",
"KC11_18","KC11_38", "KC05_11", "MC01_0", "KC11_3", "KC11_13",
"KC11_23", "KC11_0", "KC11_8", "KC11_43", "KC11_53", "KC11_68"
,"KC11_73", "KC11_48", "KC05_31", "KC11_63","KC11_58",
"KC03_0", "KC08_0", "KC05_209", "KC05_41", "KC11_83",
"KC11_88", "KC11_78" ,"KC11_93", "KC05_46", "KC11_98",
"KC11_108", "KC05_61", "KC05_51", "KC05_56", "KC05_66",
"KC11_138")

CO<-data.frame(1:46)

clusterorder<-transform(clusterorder, order=(CO))

rownames(clusterorder)=clusterorder[,1]

clusterorder$X_data=NULL

de<-merge(Stacked, clusterorder, by=0)

de_order<-order(de$X1.46)

Stacked_order<-de[de_order,]

##Plot dendrogram and bar chart of clusters##

par(mfrow=c(1,2), mar = c(2,2,2,5),oma = c(3,0,0,0),
xpd=FALSE, lty=1)

##DENDROGRAM##

plot(d1, horiz=TRUE)

mtext('Dendrogram', side=3, line=1)

mtext('Bray-Curtis Similarity', side=1, line = 3)
```

```
text(0.49,11,'Cluster 1')

text(0.49,27,'Cluster 2')

text(0.49,33,'Cluster 4')

text(0.49,39,'Cluster 3')

##BARPLOT##

##remove x=60, y=100, use Stacked_order_T[1:4,], xlim=c(0,50)
to get plot without 'OTHER' category...##

x<-c(0,10,20,30,40,50,60)

y<-c(0,10,20,30,40,50,100)

barplot(as.matrix(Stacked_order_T), las=1,  yaxt='n',
horiz=TRUE, ylab = "% Abundance", xlim = c(0,60),
labels=FALSE)

axis(1, at=x, labels = y)

legend("bottomright", legend=c("Ant.", "CD", "SA", "Other"),
fill=c("gray36", "gray49", "gray71", "gray87"), bg='white',
bty='o', text.width=8)

mtext('Relative Abundance', side=3, line=1)

mtext('% Abundance', side=1, line = 3)
```